The influence of particle concentration and composition on the fractionation of 210 Po and 210 Pb along the North Atlantic GEOTRACES transect GA03

Yi Tang, Gillian Stewart, Phoebe J. Lam, Sylvain Rigaud, Thomas Church

The influence of particle concentration and composition on the fractionation of ^{210}Po and ^{210}Pb along the North Atlantic GEOTRACES transect GA03

Yi Tang[a,b], Gillian Stewart[b,a,*], Phoebe J. Lam[c], Sylvain Rigaud[d,e], Thomas Church[d]

[a] Department of Earth and Environmental Sciences, the Graduate Center, City University of New York, New York, NY 10016, USA

[b] School of Earth and Environmental Sciences, Queens College, City University of New York, Flushing, NY 11367, USA

[c] Ocean Sciences Department, University of California Santa Cruz, Santa Cruz, CA 95064, USA

[d] School of Marine Science and Policy, University of Delaware, Newark, DE 19716, USA

[e] University of Nîmes, EA 7352 CHROME, rue du Dr. Georges Salan, 30021 Nimes, France

Corresponding author: gstewart@qc.cuny.edu

Abstract

The disequilibrium between ^{210}Po and ^{210}Pb has been used as a proxy for the particle flux from the upper ocean. The particle concentration and composition effect on the partitioning behavior of ^{210}Po and ^{210}Pb is, however, still unclear. Here, we investigate this association by comparing dissolved (< 0.45 μm) and particulate (small: 1-51 μm; large: > 51 μm) ^{210}Po and ^{210}Pb activity with size-fractionated major particle concentration and composition data from the US GEOTRACES GA03 zonal transect cruises. We observed inverse relationships between partition coefficients (K_d) for the radionuclides and the concentration of suspended particulate matter (SPM) in the water column, known as the "particle concentration effect." We examined the relationships between ^{210}Po, ^{210}Pb, and particle composition in the top 500m by using Pearson pairwise correlations for individual phases and principal components analysis (PCA) for variations among multiple phases. In addition to these analyses, an end-member mixing model was developed to estimate K_d for ^{210}Po and ^{210}Pb in the small particulate size fraction from the compositional phases. The model predicted the range of observed K_d(Pb) well, but was unable to predict the observed K_d(Po) as consistently, possibly because of the bio-reactive nature of ^{210}Po. Despite this, we found a strong relationship between ^{210}Po and both $CaCO_3$ and POM, as well as between ^{210}Pb and both opal and

lithogenic phases. All of our analyses demonstrated that the fractionation of ^{210}Po and ^{210}Pb differed between the coast and open ocean along the GA03 transect.

Keywords: *^{210}Po; ^{210}Pb; GEOTRACES; North Atlantic Ocean; particle concentration; particle composition*

1. Introduction

^{210}Po ($T_{1/2}$ = 138.4 d) and ^{210}Pb ($T_{1/2}$ = 22.3 y) are particle-reactive radionuclides in the ^{238}U decay series, produced through the decay of ^{222}Rn ($T_{1/2}$ = 3.8 d). The disequilibrium between ^{210}Po and ^{210}Pb has been used in many studies to determine particle export from the upper ocean (e.g. Buesseler et al., 2008; Friedrich and Rutgers van der Loeff, 2002; Murray et al., 2005; Shimmield et al., 1995; Stewart et al., 2007a; Verdeny et al., 2008), in a similar application to the more commonly used ^{234}Th/^{238}U system (e.g. Buesseler et al., 1992; Charette et al., 2001; Cochran, 2003). However, the fluxes of particulate organic carbon (POC) derived from these two techniques are often inconsistent and even contradictory (Buesseler et al., 2008; Friedrich and Rutgers van der Loeff, 2002; Le Moigne et al., 2013; Stewart et al., 2007a; Verdeny et al., 2008). For example, the POC fluxes derived from ^{234}Th were higher than those derived from ^{210}Po in the Polar Front region, where diatoms were dominant in the phytoplankton (Friedrich and Rutgers van der Loeff, 2002), while ^{210}Po-POC flux was greater than the ^{234}Th-POC flux in the Sargasso Sea where small phytoplankton such as *Prochlorococcus* and *Synechococcus* dominated the community (Bibby et al., 2008; Buesseler et al., 2008). In addition, POC fluxes derived from ^{210}Po were usually higher than ^{234}Th-derived estimates in the middle of gyres (e.g., Sargasso Sea, and Hawaii), whereas the opposite was generally true near the margins (Stewart et al., 2007a; Verdeny et al., 2009).

The greatest inherent differences between ^{210}Po/^{210}Pb and ^{234}Th/^{238}U have been interpreted as a result of the different half-lives of ^{210}Po and ^{234}Th, and the different particle affinities of the three particle-reactive radionuclides (^{210}Po, ^{210}Pb, ^{234}Th) (e.g. Murray et al., 2005; Verdeny et al., 2009). In particular, for the ^{234}Th/^{238}U pair, only ^{234}Th is particle-reactive while ^{238}U is highly soluble in seawater (Djogic et al., 1986). In contrast, in the ^{210}Po/^{210}Pb technique, both radionuclides are particle-reactive although they have different chemical behaviors: ^{210}Po generally has a higher affinity for particles than ^{210}Pb (Heyraud et

al., 1976; Kharkar et al., 1976). Furthermore, ^{210}Po and ^{210}Pb have different binding preferences, with ^{210}Po associated with proteins and sulfur-containing compounds (Carvalho, 2011; Fisher et al., 1983; Larock et al., 1996; Stewart et al., 2007b; Stewart and Fisher, 2003), while ^{210}Pb is adsorbed onto particle surfaces and is associated with biogenic silica and lithogenic particles (Bacon et al., 1976; Friedrich and Rutgers van der Loeff, 2002; Shannon et al., 1970; Stewart et al., 2005).

Several studies have used field collected marine material to simulate the binding behavior of Pb and Po radionuclides in the natural environment in the laboratory (Chuang et al., 2013; 2014; 2015; Yang et al., 2013). Evidence from these laboratory experiments suggests that each radionuclide binds to specific biopolymeric functional groups, with enhanced adsorption of ^{210}Po by proteins, while polysaccharides enhance the binding of ^{210}Pb (Quigley et al., 2002; Yang et al., 2013), suggesting that ^{210}Po and ^{210}Pb could be fractionated by specific organic and/or inorganic compounds during their sorption onto particles.

In this paper, we combined the measurements of ^{210}Po and ^{210}Pb in the dissolved and particulate phases, and the major phase components of suspended particulate matter (SPM) from the U.S. GEOTRACES North Atlantic transect. With these measurements, we examined the role of particle concentration and composition in the scavenging and fractionation of ^{210}Po and ^{210}Pb. The inter-correlations among the radionuclides and major particle components have also been investigated, followed by principal component analysis (PCA) aiming to reduce the number of variables to only those that are most significant in describing the variability of the data set. We also applied end member mixing analysis (EMMA (Li, 2005)) to estimate the scavenging intensities of ^{210}Po and ^{210}Pb for particles with different compositions.

2. Methods

2.1. Sampling and analysis

Seawater samples were collected at 7 “super” stations (with extra casts to provide large-volume samples) from the R/V Knorr during the US GEOTRACES North Atlantic zonal transect (NAZT), cruises KN199-04 and KN204-1. Cruise KN199-04 departed from Lisbon, Portugal in October 2010 and ended in Cape Verde in November 2010. Cruise KN204-1 departed from Woods Hole, MA in October 2011 and ended in Cape Verde in December 2011 (Fig. 1). The super stations sampled included the three stations nearest to the coasts:

stn.10-1 off Lisbon and within the influence of the Mediterranean outflow, stn.10-9 located just west of the Mauritanian shelf break, and stn.11-1 off the New England continental shelf. The other four open ocean stations were mainly located in the North Atlantic subtropical gyre, including key stations 11-10 at the BATS site, and 11-16 at the TAG hydrothermal site.

Seawater samples (~ 20 L) were collected for dissolved ^{210}Po and ^{210}Pb analysis throughout the water column at each station (12-16 depths/station) by using 30 L Niskin bottles mounted on a standard CTD rosette sampler. Particulate ^{210}Po and ^{210}Pb samples were collected using McLane in situ pumps that had been modified to accommodate two filter heads (Cutter et al., 2010; Lam et al., 2015). The paired 51 µm polyester prefilters and 1 µm quartz fiber filters (Whatman QMA) were designed to simultaneously collect large size fraction (LSF, > 51 µm) and small size fraction (SSF, 1-51 µm) particles, respectively. Details on collection and analysis of water samples and particulate matter (both small and large particulate matter) for ^{210}Po and ^{210}Pb are given in Rigaud et al. (2015). The dissolved and particulate ^{210}Po and ^{210}Pb data is available at http://www.bco-dmo.org/dataset/3914 and http://www.bco-dmo.org/dataset/3917, respectively.

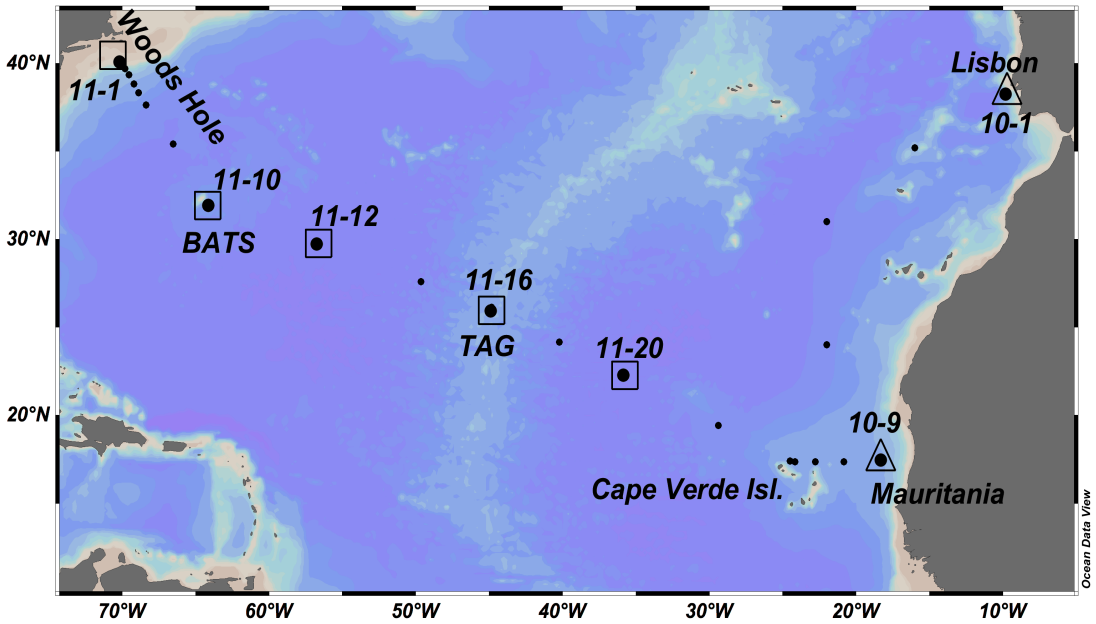

Fig. 1. Map showing stations along the US GEOTRACES GA03 North Atlantic zonal transect, from which samples were analyzed. Triangles and squares indicate stations from 2010 and 2011, respectively. BATS is the Bermuda Atlantic Time-series Site and TAG is the TAG hydrothermal site.

115 **2.2.Size-fractionated particle composition and concentrations**

116 The concentrations of six major particle compositional components (POC, $CaCO_3$, opal,
117 lithogenic matter, iron, and manganese) in both the LSF and SSF at all seven stations along
118 the transect were collected as part of the GEOTRACES NAZT project, along with basic
119 physical and chemical parameters. The details on particle sampling and particle composition
120 determination are described in Lam et al. (2015) and Ohnemus and Lam (2015). In addition,
121 the mass of suspended particulate matter (SPM) was estimated as the sum of the chemical
122 dry weight of the major particulate phases.

123 **2.3.Composition correlation and PCA**

124 The full dataset includes the activity of ^{210}Po and ^{210}Pb, and the concentration of six
125 major phase particle components including POC, $CaCO_3$, opal, lithogenic matter, Fe, and Mn
126 (Lam et al., 2015) in both SSF and LSF from the 7 "super" stations. The data matrix is
127 grouped into 2 major areas: near the continental margins (“coastal” stns.10-1, 10-9 and 11-1),
128 and in the open ocean (stns.11-10, 11-12, 11-16 and 11-20). Here we focus on the samples
129 collected from the upper 500 m depth where biological activity and aerosol deposition play
130 the most important roles in the fractionation of ^{210}Po and ^{210}Pb.

131 First, we used a Pearson pairwise correlation matrix to investigate how the size
132 fractionated particulate ^{210}Po, ^{210}Pb related to the 6 major particle components. The
133 significance of correlation coefficients, and strength of linear relationships between each pair
134 of variables was determined by 2-tailed *t*-test at $p < 0.05$. To evaluate the correlation
135 coefficient (r), we arbitrarily assign a “weak” correlation with correlation coefficient $|r| = 0.4$-
136 0.49, a “moderate” correlation with $|r| = 0.5$-0.59, and a “strong” correlation with $|r| \geq 0.6$ in
137 the following discussion.

138 We next analyzed interrelationships between particle composition measurements in the
139 SSF and LSF using a principal component analysis (PCA) for the eight variables. We applied
140 a transformation to the sample data prior to PCA by performing centering (mean subtraction)
141 and scaling (dividing the centered columns by their standard deviations). While we examined
142 the first three principal components of the PCA, the first two principal components alone
143 captured > 65% of the total variance in each dataset so the results were further visualized
144 using a biplot, which can provide inter-unit distance and indicate clustering of observations
145 as well as display variances and correlations of the variables (Kohler and Luniak, 2005).

Third, we examined the information contained in the first three principal components by regression of the principal component (PC) score of each observation against the concentration of SPM, apparent oxygen utilization (AOU), and depth. If there was a statistical relationship between PC scores and any of these parameters, we concluded that the PC was reflective of that parameter regardless of the nature of the relationship. Because the signs of PC scores are arbitrary and the data has been transformed, whether the relationship is positive or negative, linear or non-linear has no significance to our interpretation.

2.4. Partition Coefficients Analyses

The partition coefficients (K_d) of ^{210}Po and ^{210}Pb are useful for describing their affinity to marine particles (Bacon et al., 1976; Baskaran and Santschi, 1993; Wei and Murray, 1994). The interpretation of the K_d(Po) is complicated because while ^{210}Pb only adsorbs to the surface of particles, ^{210}Po is both sorbed to surfaces and also taken up into the cytoplasm of phytoplankton cells and bioaccumulated through food chains (see Discussion for further explanation). Even though the interactions of ^{210}Po and ^{210}Pb with particles are not the same, we will use "adsorption" or "sorption" for both ^{210}Po and ^{210}Pb to describe their particle association in this paper.

K_d (L kg^{-1}) is defined as:

$$K_d = \frac{A_p}{A_d} \times \frac{1}{SPM} \quad (1)$$

where A_p and A_d represent the nuclide activities in the particulate and the dissolved phases (dpm 100L^{-1}), respectively, and SPM is the suspended particulate matter concentration (μg L^{-1}). K_d provides a measure of the partitioning of radionuclides between the dissolved and particulate phases. The conceptualized scavenging models consider chemical interactions between radionuclides either (1) in the dissolved and total particulate phases (two-box model) or (2) in the dissolved – small – large particulate phases (three-box model) or (3) in the truly dissolved – colloidal – small – large particulate phases (Baskaran et al., 1992; Clegg and Whitfield, 1991; 1990; Rigaud et al., 2015; Savoye et al., 2006). We calculated the coefficients of the bulk partitioning between the dissolved and small particulate phases (K_d_SSF), and between the dissolved and total particulate phases (K_d_TOT) without considering colloidal phase due to lack of data. However, in our samples over 90% of the total particulate radionuclide activity was in the small size fraction, and therefore these K_d values were very similar. We will only present the K_d_SSF in this paper.

Next, we examined the degree to which ^{210}Po and ^{210}Pb are fractionated during sorption. The fractionation factor (F), a ratio of the corresponding bulk K_d's (Chase et al., 2002; Murray et al., 2005; Nozaki et al., 1998),

$$F(Po/Pb) = K_d(Po)/K_d(Pb) \quad (2)$$

was used to investigate the preferential sorption of ^{210}Po relative to ^{210}Pb.

Furthermore, in order to interpret the relationship between particle composition and the bulk partition coefficients, a six-end-member mixing model was developed here similar to the one published by Hayes et al. (2015) for thorium isotopes.

$$K_d = \sum_1^6 (K_d)_i \cdot f_i = (K_d)_1 \cdot f_1 + (K_d)_2 \cdot f_2 + (K_d)_3 \cdot f_3 + (K_d)_4 \cdot f_4 + (K_d)_5 \cdot f_5 + (K_d)_6 \cdot f_6 \quad (3)$$

where K_d is the observed bulk partition coefficient of a given nuclide, $(K_d)_i$ is the partition coefficient for pure end member i, f_i is the proportion of end member i of the total mass of a particle sample, where i = 1 (POM), 2 ($CaCO_3$), 3 (opal), 4 (lithogenic material), 5 (Fe), 6 (Mn). Eq. (1) and (3) were formatted for each particle sample, and therefore for a set of given $i = n$ samples, f_i (n×6 matrix) and K_d^i (n×1 matrix) are all known. The unknown $(K_d)_i$ (6×1 matrix) can be solved by Eq. (4) using non-negative least squares regression (since the negative K_d has no physical meaning).

$$\begin{bmatrix} f_1^1 & f_2^1 & f_3^1 & f_4^1 & f_5^1 & f_6^1 \\ f_1^2 & f_2^2 & f_3^2 & f_4^2 & f_5^2 & f_6^2 \\ f_1^3 & f_2^3 & f_3^3 & f_4^3 & f_5^3 & f_6^3 \\ & & & \dots & & \end{bmatrix} \times \begin{bmatrix} (K_d)_1 \\ (K_d)_2 \\ (K_d)_3 \\ (K_d)_4 \\ (K_d)_5 \\ (K_d)_6 \end{bmatrix} = \begin{bmatrix} k_d^1 \\ k_d^2 \\ k_d^3 \\ \dots \end{bmatrix} \quad (4)$$

We estimated the standard error of the derived end-member K_d values using the jackknife resampling technique (Efron and Stein, 1981). Finally, the derived end-member fractionation factors, F(Po/Pb), were calculated from Eq. (2) for each compositional component.

3. Results

3.1. Correlations

In the open ocean, ^{210}Po activity was strongly correlated with POC and moderately correlated with $CaCO_3$ in the small particles, and ^{210}Po activity in the large particles was strongly correlated with $CaCO_3$, moderately correlated with opal, and weakly correlated with POC (Table 1). ^{210}Pb activity in the open ocean, in contrast, was moderately correlated with

$CaCO_3$, opal, and Mn in the large particles but there were no significant correlations with ^{210}Pb activity in the small particles. In the coastal waters, both ^{210}Po and ^{210}Pb activities in the large particles were strongly correlated with POC, $CaCO_3$, and opal. ^{210}Po and ^{210}Pb activities in the small particles near the coasts, however, had different relationships with the 6 particulate components relative to those in large particles. For instance, ^{210}Pb activity strongly correlated with opal and Mn, and moderately correlated with lithogenic matter and Fe near the coasts whereas ^{210}Po activity was found to be strongly correlated with lithogenic matter and Fe.

Table 1. Pairwise Pearson Correlation Coefficients, r, within size-fractionated principal particle compositions in the top 500 m at coastal (stns.10-1, 10-9 and 11-1) and open ocean (stns.11-10, -12, -16 and -20) stations. Bold values with * and ** denote moderate and strong correlation with $p < 0.05$ by *t*-test, respectively.

	Coasts				Open Ocean			
	SSF (n = 19)		LSF (n = 18)		SSF (n = 20)		LSF (n = 19)	
	^{210}Po	^{210}Pb	^{210}Po	^{210}Pb	^{210}Po	^{210}Pb	^{210}Po	^{210}Pb
POC	0.05	0.07	**0.68****	**0.60****	**0.68****	0.30	0.45	0.18
$CaCO_3$	0.25	0.44	**0.72****	**0.65****	**0.59***	0.42	**0.71****	**0.59***
Opal	-0.01	**0.64****	**0.76****	**0.70****	0.18	-0.14	**0.53***	**0.50***
Litho	**0.75****	**0.54***	0.07	0.05	-0.06	-0.01	0.34	0.10
Fe	**0.74****	**0.56***	0.08	0.07	-0.03	0.00	0.15	-0.05
Mn	0.36	**0.84****	0.43	0.42	-0.47	-0.11	0.34	**0.58***

Overall, the correlations between the particle components and ^{210}Po and ^{210}Pb activity in the large particles were reasonably consistent between coastal and open ocean samples, whereas the corresponding correlations in the small particles varied between those two oceanic provinces.

3.2. Principal Component Analysis

Principal component analysis (PCA) was applied to all eight measured variables to identify a new set of fewer, uncorrelated variables that can explain a substantial portion of the variation of the original variables. The new set of variables, also called the principal components (PC), will result in a lower dimensional space that explains most of the variation. We analyzed all the SSF data and all the LSF data as two datasets, and PCA results were summarized in Table 2, including the loadings of the first three principal components (total 8 principal components) and their contribution in explaining of the total variance. In the SSF

dataset (Table 2, SSF), the first three principal components contained 76.9% of the variation of the eight original variables, with 49.8% explained by PC1, 14.8% explained by PC2, and 12.3% explained by PC3. The highest loadings of PC1 were from Mn, Fe, $CaCO_3$ and lithogenic matter, PC2's highest loadings were ^{210}Po and POC, whereas lithogenic matter and Fe were most important to PC3 (Table 2, Fig. 2).

Table 2. The first three principal component loadings, percentage of variance explained by each principal component, and their cumulative percentage of total variance in the small size fraction (SSF) and the large size fraction (LSF) of the particles. The numbers in bold font indicate the absolute loadings that are higher than 0.4.

	Variables	PC1	PC2	PC3
SSF (1-51 µm)				
	^{210}Po	-0.001	**0.858**	0.070
	^{210}Pb	-0.226	0.118	-0.149
	POC	-0.279	**0.427**	-0.245
	$CaCO_3$	**-0.414**	0.056	-0.286
	Opal	**-0.401**	-0.205	**-0.406**
	Litho	**-0.412**	-0.023	**0.570**
	Fe	**-0.417**	-0.034	**0.553**
	Mn	**-0.441**	-0.146	-0.187
	% of Variance	49.8	14.8	12.3
	Cumulative %	49.8	64.6	76.9
LSF (> 51 µm)				
	^{210}Po	**-0.408**	-0.110	**0.466**
	^{210}Pb	-0.396	-0.070	**0.593**
	POC	-0.362	-0.292	**-0.493**
	$CaCO_3$	**-0.405**	-0.239	-0.324
	Opal	-0.386	-0.321	-0.121
	Litho	-0.243	**0.536**	-0.195
	Fe	-0.249	**0.532**	-0.163
	Mn	-0.334	**0.409**	0.058
	% of Variance	59.9	29.8	7.4
	Cumulative %	59.9	89.7	97.1

In contrast, the first three components of the LSF dataset explained 97.1% of the total variance, in which PC1 explained 59.9%, PC2 explained 29.8%, and PC3 explained 7.4% (Table 2, LSF). We observed that the highest PC1 loadings came from ^{210}Po and $CaCO_3$,

PC2's highest loadings were from lithogenic matter, Fe, and Mn, and PC3 loadings were mainly from ^{210}Po, ^{210}Pb and POC (Table 2, Fig. 2).

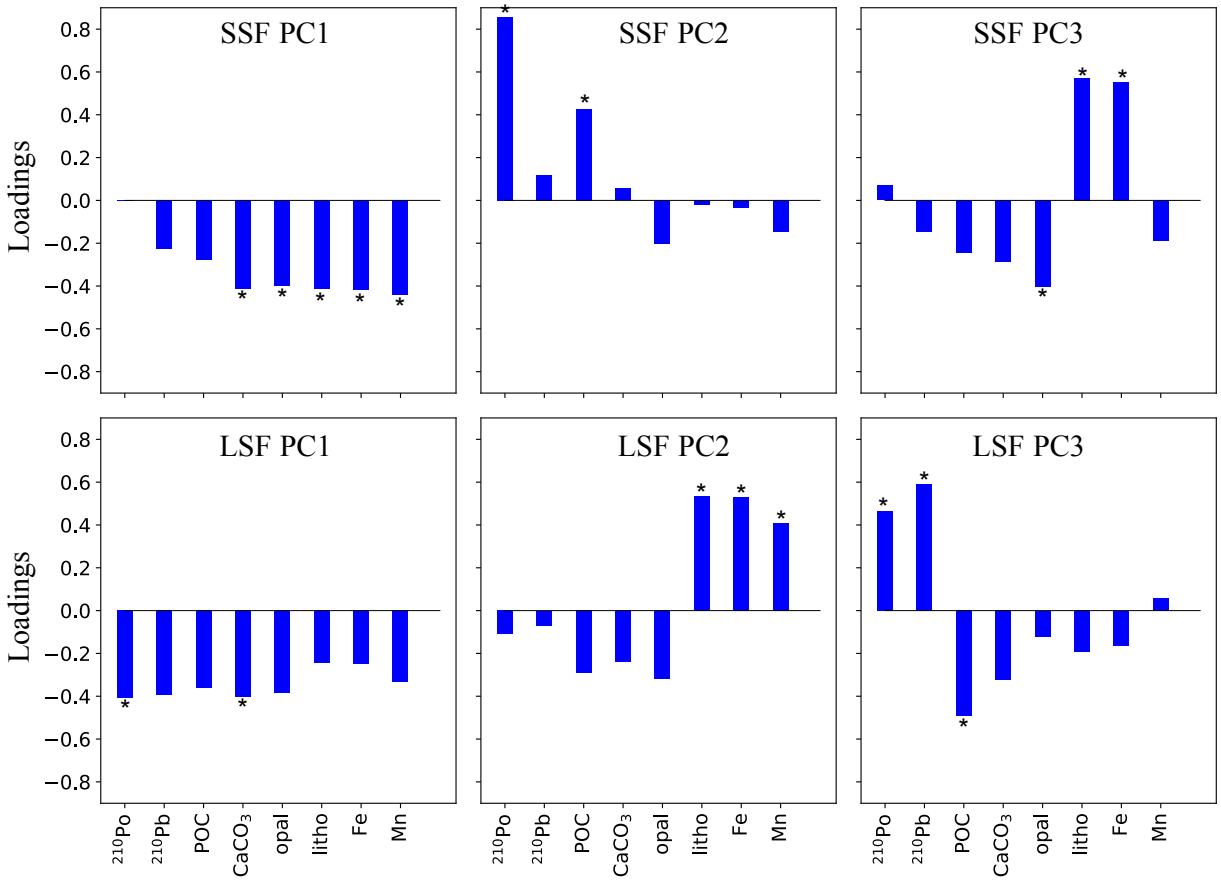

Fig. 2. The first three principal component loadings with respect to each variable in the small size fraction (SSF) and the large size fraction (LSF) of the particles. The symbol "*" indicates the absolute loadings that are higher than 0.4.

Further, PC1 and PC2 scores of the observations for each station were examined and visualized using biplots (Fig. 3). In the SSF dataset, the observations in the open ocean stations generally scored high and positive on PC1, whereas the SSF at coastal station 11-1 scored high on PC1 but with negative values. The observations at stn.10-9, on the other hand, had little loading from PC1, but had some variability along PC2, with generally negative scores. Three of the very shallow (~ 40 m) open ocean observations scored relatively high and positive on PC2 (stn.11-12, 11-16, and 11-20) (Fig. 3A). Most observations at stn.10-1 scored rather equally on PC1 and PC2, except for one observation (30 m) with significant

negative scores on PC1, suggesting this observation was overwhelmingly explained by this component.

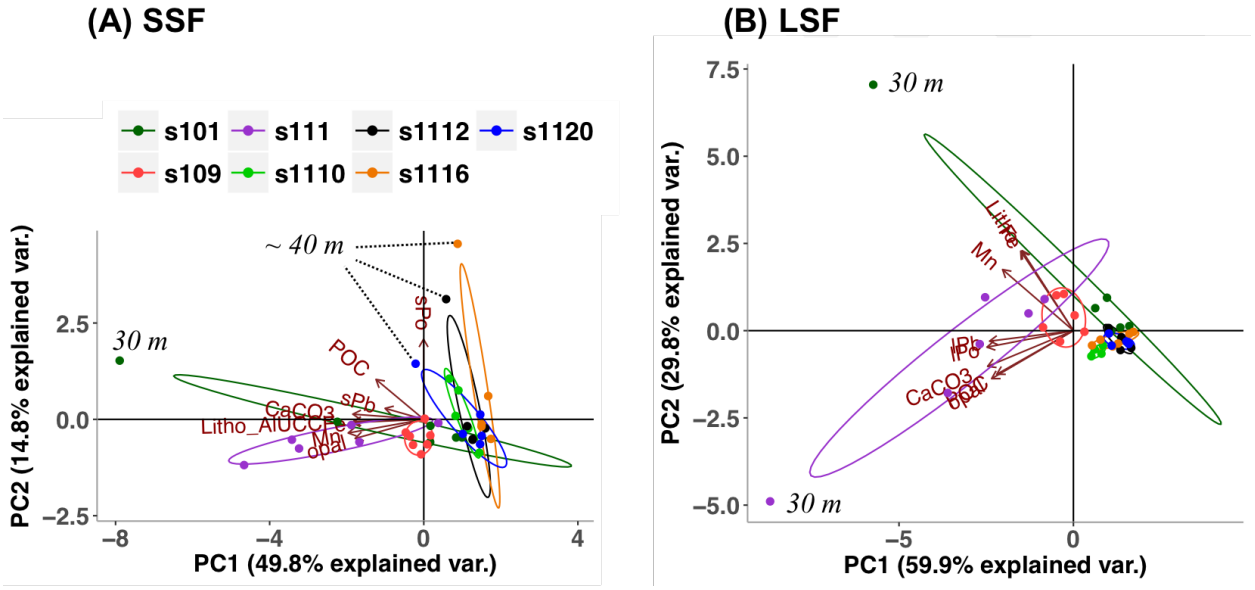

Fig. 3. Biplots of principal component (PC1 and PC2) scores based on observations for each station. A: small size fraction (SSF); B: large size fraction (LSF). PC1: first principal component, PC2: second principal component. The color of each point indicates samples from a particular station number, and ovals denote the clustering of those samples. Note that the scales of A and B are different and the depths of the extreme points are annotated (see section 3.2 for detailed description).

In the LSF dataset, the observations in the open ocean stations mostly scored highly positive on PC1 (Fig. 3B). The PC1 scores for the observations at stn.10-1 were generally higher than PC2 scores (positive), except from the observation at 30 m, which was the only observation from this station to have a strongly negative PC1 score and also had a much higher (positive) score on PC2 compared to the rest of the samples at this station. At stn.10-9, the surface observations had generally negative scores on PC1, and the observations below the surface layer had generally positive scores on PC2. The observations at stn.11-1, on the other hand, scored highly negative on PC1, especially the observation at 30 m.

Looking at each biplot (SSF and LSF separately), component scores for the four open ocean stations in both plots displayed a clustered pattern, whereas the observations for the three coastal stations were more varied along PC1 and PC2. Despite the fact that the principal components may represent different causes of variability between SSF and LSF, this suggests

more uniform open ocean particle characteristics within each size fraction, but more diverse particle characteristics at the coasts. Additionally, we observed several extremely high scores in a few surface samples (samples annotated on Fig. 3), indicating those observations were overwhelmingly explained by a single component.

3.3.The bulk partition coefficients of ^{210}Po and ^{210}Pb

The K_d values for ^{210}Po in the SSF varied between 0.10 and 2.12 $\times 10^7$ L kg^{-1} (median: 0.43$\times 10^7$ L kg^{-1}). In contrast, the K_d values for ^{210}Pb ranged from 0.05 to 0.89 $\times 10^7$ L kg^{-1}, with a median value half as large as that of ^{210}Po in the SSF (Fig. 4). We also noticed different regional patterns in K_d for both ^{210}Po and ^{210}Pb between the coasts and open ocean. For instance, K_d for ^{210}Po in the SSF in the three stations nearest to the coasts (filled markers) were 2-times lower than those in the remote regions of the ocean (open markers) (Fig. 4A). The K_d(Pb) values, on the other hand, showed higher values between 50 and 150 m near the coastal margins than in the interior ocean (Fig. 4B).

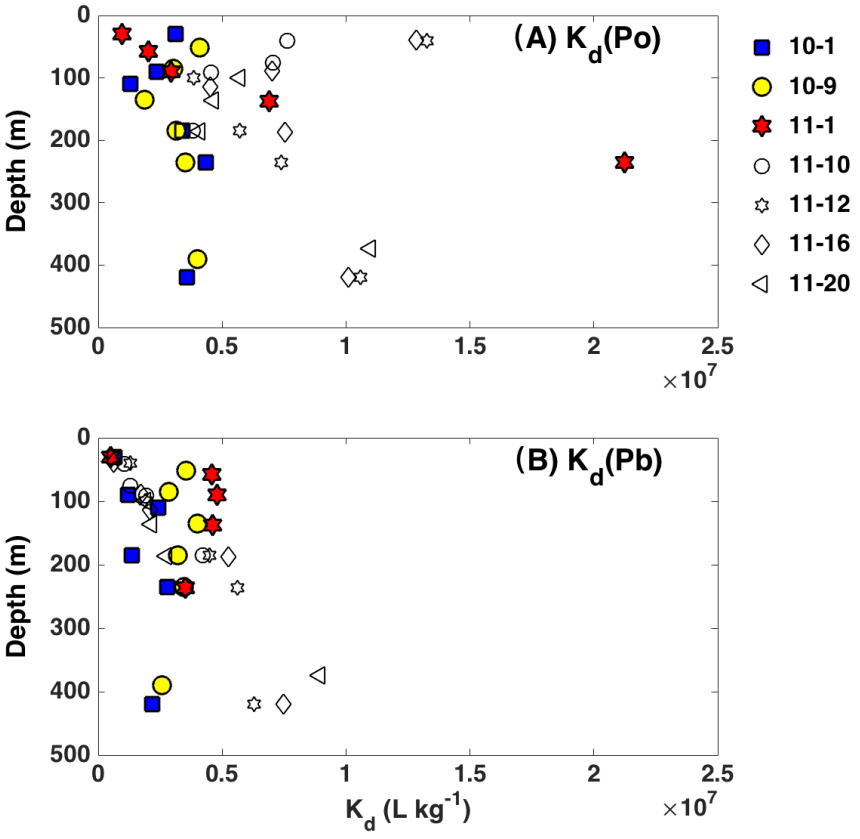

Fig. 4. Partition coefficient (K_d in the unit of L kg^{-1}) of ^{210}Po and ^{210}Pb with marine suspended particulate matter (SPM) in the upper 500 m along the NAZT GA03 transect. (A): K_d of ^{210}Po in the small size

297 fraction (1-51 μm). (B): K_d of ^{210}Pb in the small size fraction. The filled markers indicate the three stations
298 nearest to the margins (stns.10-1, 10-9, 11-1) and the open markers indicate the four open ocean stations
299 (stns.11-10, -12, -16, -20).
300
301 **3.4.Fractionation between ^{210}Po and ^{210}Pb in the bulk samples**
302 The fractionation factor of the bulk sample, F(Po/Pb), which is the ratio of the bulk
303 K_d(Po) to bulk K_d(Pb), ranged from 0.44 to 20.5 in the small particles (Fig. 5). We observed
304 that the fractionation factor generally decreased with depth at nearly all stations, displaying a
305 F(Po/Pb) minimum in the subsurface zone between 100-200 m. For the particles collected
306 from the interior ocean, F(Po/Pb) were all greater than 1 in the upper 300 m, indicating a
307 strong preference for scavenging of ^{210}Po over ^{210}Pb. In contrast, F(Po/Pb) values for
308 particles near the coasts reveal that most were lower than or equal to unity, indicating a slight
309 preference for scavenging of ^{210}Pb over ^{210}Po, or perhaps a higher rate of ^{210}Po
310 remineralization from the particles to the seawater (Rigaud et al., 2015).
311

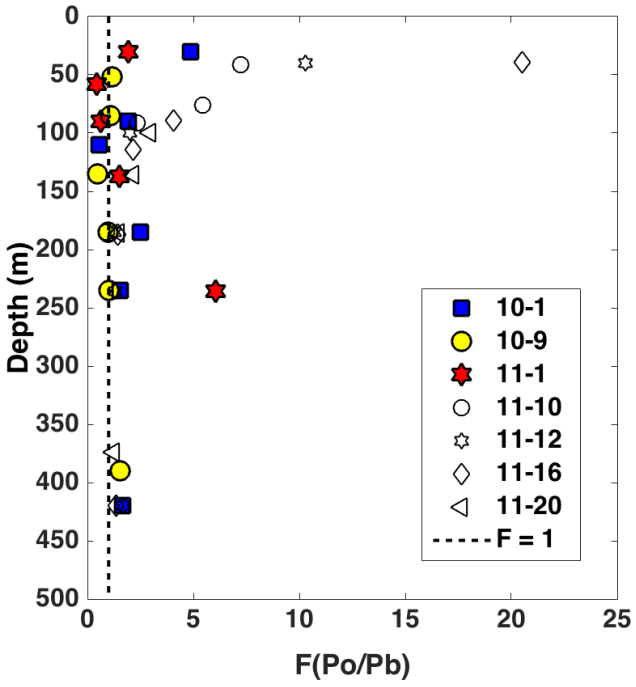

312
313 Fig. 5. Fractionation of ^{210}Po relative to ^{210}Pb (F(Po/Pb) = K_d(Po)/K_d(Pb)) in the small size fraction. The
314 vertical dashed line is drawn for F = 1. The filled markers indicate the three stations nearest to the margins
315 (stns.10-1, 10-9, 11-1) and the open markers indicate the four open ocean stations (stns.11-10, -12, -16, -
316 20).
317

4. Discussion

4.1. Correlations of radionuclide activities to chemical composition

We observed correlations between ^{210}Po activity and POC in the large particles across both the coastal and open ocean stations, while similar correlations in the small particles were only found in the open ocean but not in coastal waters (Table 1). When correlations existed between ^{210}Po activity and POC in the upper 500 m, there were also correlations between ^{210}Po activity and $CaCO_3$. In our PCA results, POC and $CaCO_3$ in the large particles had similar loadings on the first three principal components while the loadings of POC and $CaCO_3$ in small particles had similar values on PC1 and PC3, but not on PC2 (Table 2, Fig. 2). These results suggest that POC and $CaCO_3$ were more closely associated with each other and more evenly important to the components in the large particles relative to their relationship in the small particles. Indeed, correlations between POC and $CaCO_3$ were previously observed in the large particles in the upper 2000 m in this section, but no such correlations were seen at any depth in the small particles (Lam et al., 2015). This may be due to a relationship between "ballast" $CaCO_3$ and POC in large, sinking particles (Armstrong et al., 2001).

Despite these relationships in the large particles, in the small particles near the margins no correlation was found between ^{210}Po and POC, while strong positive relationships were observed between ^{210}Po and Fe and lithogenic material (Table 1). As these areas had the highest input of lithogenics (Lam et al., 2015), we suggest that this could reflect scavenging of ^{210}Po by particles from atmospheric dust deposition or continental shelf input. This is an indication that the source of particles can influence the distribution of ^{210}Po, and suggests that the radionuclide activity in the small particles near the coasts has a different relationship with Fe and lithogenic phases than the small particles and large particles in the rest of the study.

While large particles are often aggregates of small particles in the surface ocean, the large particles throughout the water column (top 500m) at the coasts and open ocean had different correlations between the compositional components and ^{210}Po and ^{210}Pb than the small particles, implying that they are not just aggregates of smaller particles. Below the surface layer, there are many reasons to explain why various sized particle compositions could be different (explained further in 4.2).

348 It was reported by Friedrich and Rutgers van der Loeff (2002) that the fractionation of
349 ^{210}Po and ^{210}Pb on particles from the Antarctic Circumpolar Current was dependent on the
350 POC/opal ratio, and suggested that ^{210}Po was more strongly associated with POC while ^{210}Pb
351 was more associated with opal. The Pearson correlation analysis in this study (Table 1)
352 revealed a stronger correlation between POC and ^{210}Po than between POC and ^{210}Pb in
353 general. The results did not show a stronger correlation between opal and ^{210}Pb than between
354 opal and ^{210}Po.
355

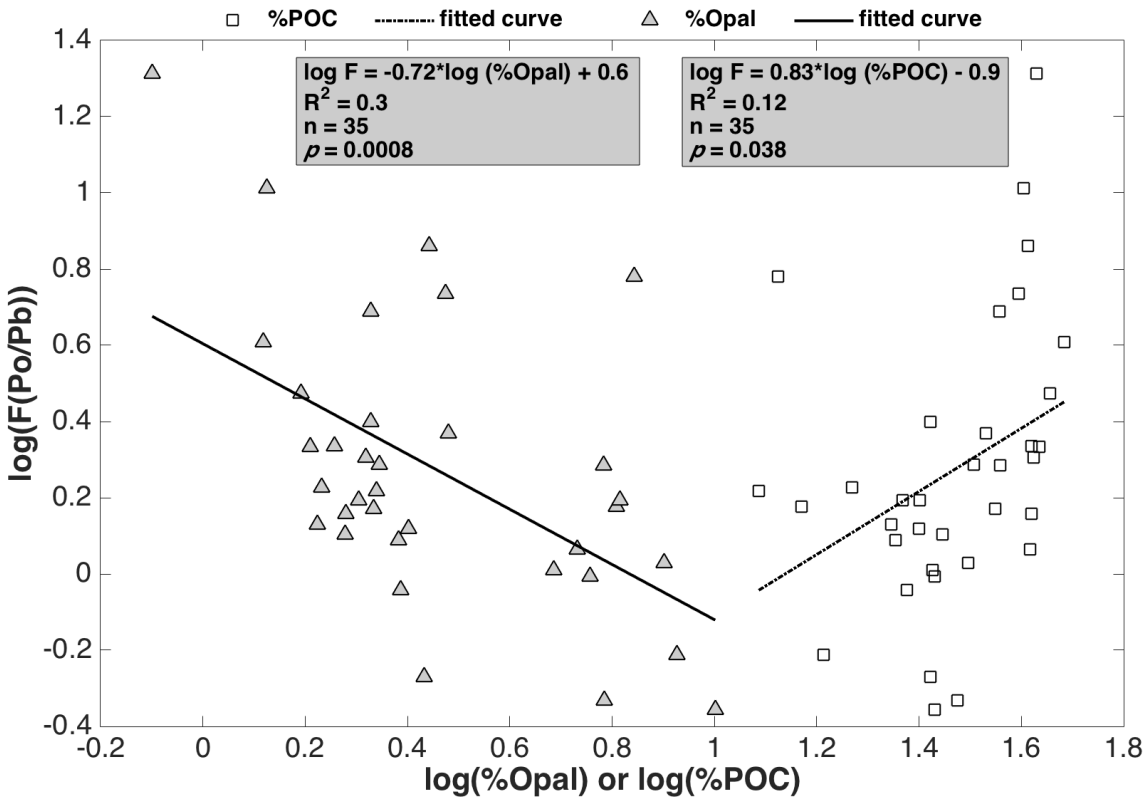

356
357 Fig. 6. The log-log model: $\log F(Po/Pb) = \alpha + \beta \log(\%opal)$ and $\log F(Po/Pb) = \alpha + \beta \log(\%POC)$ was
358 applied to study the linear relationship between the logarithmic transformed dependent and independent
359 variables. Open squares represent log(%POC), and filled triangles indicate log(%opal). The curves were fitted
360 by linear regression functions, and the fitted function and corresponding statistical information are shown in the
361 gray-shaded boxes.
362
363 To examine this further, we applied linear regression models by plotting log(F(Po/Pb))
364 against both log(%POC) and log(%opal) for small particles (Fig. 6). This was done only for
365 small particles because we only calculated K_d(Po) and K_d(Pb) for these particles. A linear

function fit the relationship between log(F(Po/Pb)) and log(%opal) reasonably well (R^2 = 0.29, n = 35, p = 0.0008), showing a 1% increase in %opal reduces F(Po/Pb) by 0.7%, supporting siliceous matter's preferential affinity for ^{210}Pb. The relationship between log(F(Po/Pb)) and log(%POC), on the other hand, was not well captured with a linear function (R^2 = 0.13, n =35, p = 0.04). Nonetheless, the relationship is still significant, suggesting a 1% increase in %POC increases F(Po/Pb) by 0.8%, supporting the association of ^{210}Po with POC.

We did, however, find lower F(Po/Pb) values in surface samples from the coasts than we found in the open ocean, despite the higher POC along the margins (Figure 5). It is worth noting that the phytoplankton composition near the coasts was dominated by siliceous plankton (diatoms, higher %opal) (Twining et al., 2015a), and could result in a decrease in F(Po/Pb), despite high %POC. To further assess this, we applied a multiple linear regression by using both log(%opal) and log(%POC) as predictors and log(F(Po/Pb)) as response: log(F(Po/Pb)) = 0.0155 - 0.63733 log(%opal) + 0.37465 log(%POC) (R^2 = 0.31). The results suggest that %opal has a larger negative impact and %POC had a smaller positive impact on the fractionation. When %opal and %POC are combined in the model, log(%POC) is no longer significant (p = 0.33) while log(%opal) is (p = 0.005). Due to this smaller fractionation between ^{210}Po and ^{210}Pb near the margins, the ^{210}Po deficits with respect to ^{210}Pb were not as significant as those in the subtropical gyre (Rigaud et al., 2015) where non-siliceous organisms like *prymnesiophytes*, *cryptophytes* and *chrysophytes* comprised 40-60% of the community (Twining et al., 2015a).

4.2.Interpretation of PCA

According to the PCA loadings (Fig. 2) and scores in the biplots (Fig. 3), the first principle component (PC1) for both the SSF and the LSF was characterized by similar loadings of the compositional components (all negative) as well as a clear geographic split in sample scores; samples from the open ocean had positive scores, samples from the coastal stations had generally negative scores, and samples from station 10-9 had a unique distribution with both negative and positive scores. Both of these observations suggest a similar interpretation for PC1 for both size fractions. In contrast, the loadings and scores for PC2 were distributed quite differently between SSF and LSF samples, suggesting a different interpretation for this PC in the SSF vs. LSF. In addition, the loadings and scores (data not

shown) for PC3 were also distinct between the two size fractions, but there were some similarities between the loadings of PC3 in the SSF and PC2 in the LSF. The loadings for PC2 in the SSF and PC3 in the LSF were relatively distinct from all the other loading patterns.

To attempt to interpret the "meaning" of the first three principle components in each size fraction, we plotted the scores of all the samples against physical and chemical characteristics of the samples from the GEOTRACES database. For example, because the scores on PC1 of both size fractions seemed to be related to geographic distribution, but the loadings of all the variables were similar/negative, we expected that some trend other than particulate composition was driving this component from the coast to the open ocean. We hypothesized that this could be related to total suspended particle load (SPM), which tends to be higher at margin stations. Along the transect, between 52 and 99% of the mass of SPM was determined by three biogenic phases: POM (which is 1.88 × POC), opal, and $CaCO_3$ (data not shown), which all are generated by phytoplankton production. Thus, SPM could be used as an indicator of production, with a gradient from the coast to the center of the gyre. Indeed, we observed a strong and significant linear relationship between PC1 scores and the concentration of SPM in both the small and large size fractions (SSF: $R^2 = 0.66$; LSF: $R^2 = 0.73$) (Fig. 7A), suggesting a similar interpretation ("production") for PC1 in both size fractions. However, no general pattern was found using SPM as an explanatory variable for the variations in PC2 or PC3 in both size fractions.

PC2 has strong positive loadings for both ^{210}Po and POC in the SSF (Table 2, Fig. 2) and we hypothesized that this PC was related to some biogeochemical processes that affected ^{210}Po and POC in a similar manner in the SSF. We did in fact find a strong relationship by using a two-term exponential model ($R^2 = 0.45$) between PC2 in the SSF and apparent oxygen utilization (AOU) (Fig.7B), while none of the other PCs had a significant relationship with AOU. AOU is defined as the difference between the saturation oxygen concentration and the observed oxygen concentration. Dissolved oxygen in the seawater is consumed by microorganisms for the oxidation of organic matter, and therefore AOU can be used as a measure of respiration/remineralization in the oceans (Duteil et al., 2013; Ito et al., 2004). Besides reflecting local respiration/remineralization, AOU is also related to water mass age and the ventilation age of the water (Stanley et al., 2012). This relationship between PC2 in

small particles, which has the highest loadings from ^{210}Po activity, and AOU suggests that recent and past remineralization and respiration affect the ^{210}Po distribution in small particles more than large particles.

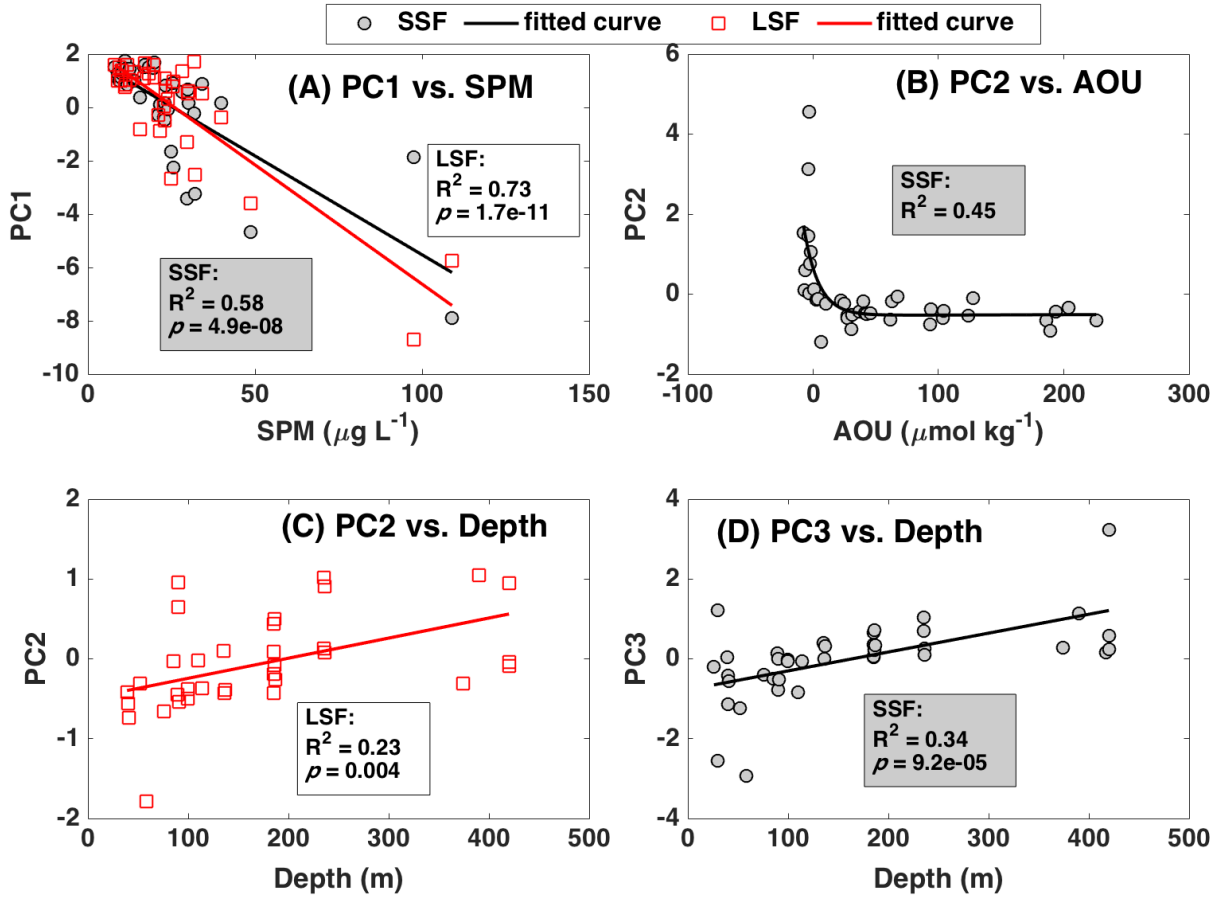

Fig. 7. Relationships between the scores on the first three principal components and the concentration of suspended particulate matter (SPM), apparent oxygen utilization (AOU), and depth. There were a total 9 relationships in each size fraction: PC (1, 2, 3) vs. SPM, PC (1, 2, 3) vs. AOU, and PC (1, 2, 3) vs. Depth. Only the graphs with significant relationships are displayed in this figure: (A) PC1 score vs. SPM (SSF and LSF); (B) PC2 score vs. AOU (SSF); (C) PC2 score vs. Depth (LSF); (D) PC3 score vs. Depth (SSF). The filled gray circles represent the SSF and open red squares represent the LSF. The statistical regression lines (solid line) and the R-squared statistic (R^2) are shown in all the plots. The *p*-value is annotated only for linear regressions (A, C, D) but not for the two-term exponential model (B).

Looking at the loadings further (Table 2, Fig. 2), it seems that SSF PC3 (12.3% variation explained) and LSF PC2 (29.8% variation explained) could be driven by similar variables,

and appear to reflect a gradient from biogenic particle phases (POC, $CaCO_3$, opal), which have negative loadings, towards abiotic particle phases (litho, Fe, Mn), which have positive loadings. This transition from biogenic material towards inorganic mineral phases tends to occur as freshly-produced particles sink from the surface and degrade with depth. Indeed, when the scores along these principle components were plotted vs. depth, the relationship for both was linear and significant (Fig. 7C and 7D). There were no significant relationships between PC3 and any of the variables we examined in the large size fraction.

The different relationships between principle components and production and remineralization suggests a decoupling of the driving forces that determine composition and ^{210}Po and ^{210}Pb activity in the two size fractions, suggesting both different sources and possibly different residence times between the SSF and the LSF in the top 500m. For example, the source of LSF may reflect production in the surface ocean, especially at the margins where large diatoms, foraminifera, and pteropods could be predominating. The source of SSF in the surface, on the other hand, is probably composed of small diatoms and flagellates. Further differences between the particle characteristics may reflect differences in the residence times of large (faster sinking) and small (slower sinking) particles, especially below the euphotic zone. While there is evidence that large particles are often aggregates of small particles in the surface (Ohnemus and Lam, 2015), there is no reason to expect their compositions will be identical, especially as particles leave the euphotic zone. Small particles at depth may be derived from the disaggregation of larger particles, and may spend several months in the water column as they sink slowly. In contrast, large particles at the same depths could represent fast-sinking material that left the surface within the past several days-weeks, and so may be "fresher" than the small particles in this study due to differences in the extent of degradation and remineralization (Abramson et al., 2010; Wakeham and Canuel, 1988).

Stewart et al. (2007b) applied principal component analysis to explore the connection between ^{210}Po and organic matter within sediment trap particles at 200m in the northwestern Mediterranean. They suggested that degradation contributed the most to the variability in the composition of those sinking particles. While we find remineralization (low AOU as a proxy for "freshness") was an important driver of variation in the small particles, it was not significant for the large particles. The difference in our results, specifically the lack of

correlation between AOU and PC scores for large particles, may be caused by differences between the particulate material collected by sediment traps and those collected by in situ pumps (Abramson et al., 2010; Lepore et al., 2009). This concept, however, that degradation and sinking speed can cause some variation of composition within the small and large particles, was confirmed by our result that the depth of the sample is correlated to the distribution along PC2 in the large fraction (which explains 30% of the variation in the particle composition), and along PC3 in the small fraction (12 % of the variation). Thus differences between our results and those of Stewart et al. (2007b) could also be explained by the range of depths of our samples (0-500 m) as opposed to the single depth (200 m) of the sediment trap.

4.3.Particle concentration effect

The K_d values suggest that ^{210}Po has a higher affinity for particles than ^{210}Pb, as its K_d ranged between $10^{6.0}$ and $10^{7.3}$ L kg^{-1} while the K_d values for ^{210}Pb ranged from $10^{5.7}$ to$10^{7.0}$ L kg^{-1}. These K_d values are higher and span a wider range compared to previous values in the nearshore waters off western Taiwan ($10^{5.53}$-$10^{5.56}$ and $10^{5.38}$-$10^{5.87}$ L kg^{-1}, Wei et al., 2012), in surface waters of the northwestern Mediterranean Sea ($10^{5.80}$-$10^{5.97}$ and $10^{4.90}$-$10^{5.08}$ L kg^{-1},Masqué et al., 2002), and in the turbid waters of the Yellow Sea ($10^{4.59}$-$10^{6.51}$ and $10^{5.23}$-$10^{5.86}$ L kg^{-1}, Hong et al., 1999). All the samples collected in these previous studies were either from surface waters or coastal, turbid environments. The samples evaluated in our study, in contrast, were collected from the surface to 500 m depth, and from the coast to the open ocean, covering a wider range in SPM concentration and more diverse particle composition. Indeed, an even wider range of K_d(Po) values ($10^{4.7}$-$10^{7.2}$ L kg^{-1}) and K_d(Pb) values ($10^{5.0}$-$10^{6.8}$ L kg^{-1}) was observed in a 4000-m water column study in the northern South China Sea (Wei et al., 2014).

We examined the effect of particle concentration on the solid/solution partitioning for ^{210}Po and ^{210}Pb by focusing on the uptake of radioactivity from the water to the small particles. The values of partitioning (log K_d) versus particle concentration (log SPM) in the small particles are shown in Fig. 8. Over a range of more than two orders of magnitude of SPM concentrations, an inverse correlation between log K_d and log SPM was observed for both ^{210}Po and ^{210}Pb in this study. Such negative correlation, known as the "particle concentration effect", has been commonly found in field and laboratory observations for ^{210}Po, ^{210}Pb, and

other particle-reactive radionuclides such as ^{230}Th, ^{234}Th, ^{231}Pa, and ^{7}Be (Hayes et al., 2015; Wei and Murray, 1994). Although a number of hypotheses have been proposed to explain this observation, the presence of colloidal material which scavenges radionuclides is widely accepted as the factor that results in the particle concentration effect (Honeyman et al., 1988; Honeyman and Santschi, 1989). The colloids provide sorption sites available for particle-reactive species within the operationally defined "dissolved" phase. Increases in particle concentration are associated with increases in the amount of colloidal radionuclides (Benoit and Rozan, 1999). The colloidal radionuclide passes through the 0.45 μm filters and will result in an overestimate of the dissolved radionuclide fraction (A_d) in the water column (Li, 2005) as well as lower K_d and hence the inverse relationship between log K_d and log SPM. Recent work on the kinetics of thorium scavenging has suggested that the particle concentration effect could also be explained by a dependency of the loss of thorium from the particle phase (e.g., by desorption and/or remineralization) on particle concentration (Lerner et al., 2017) but it is unknown whether this would also apply to ^{210}Po and ^{210}Pb. The slope of the log K_d vs. log SPM plot observed for the entire dataset was -0.54 ($R^2 = 0.22$, $p = 0.004$, n =35) for ^{210}Po and -0.83 for ^{210}Pb ($R^2 = 0.47$, $p < 0.0001$, n = 35). This finding is comparable with the slope of -0.79 for ^{210}Po and -0.78 for ^{210}Pb in the East China Sea (Su et al., 2016), but the slopes of the regression lines are flatter than the values reported in the water column at Kuala Selangor, Malaysia (-1.05 for ^{210}Po and -1.20 for ^{210}Pb) (Theng and Mohamed, 2005).

This relationship was further examined for coastal and open ocean stations respectively, and the results show some regional differences. We found a significant negative relationship between log K_d(Po) and log SPM in the coastal waters ($R^2 = 0.24$, $p = 0.04$), whereas no significant linear correlation was observed in the open ocean (Fig. 8A). In contrast, log K_d(Pb) was significantly correlated with log SPM in the open ocean ($R^2 = 0.91$, $p < 0.0001$) but not at the coastal stations (Fig. 8B). It is also worth noting that the log K_d values for ^{210}Po near the coasts tended to be lower at a given particle concentration (SPM: ~ 10- 25 μg L^{-1}) than would have been expected based on the data from the open ocean. In contrast, most log K_d values for ^{210}Pb near the coasts were higher than those observed in the open ocean at the same range of particle concentration.

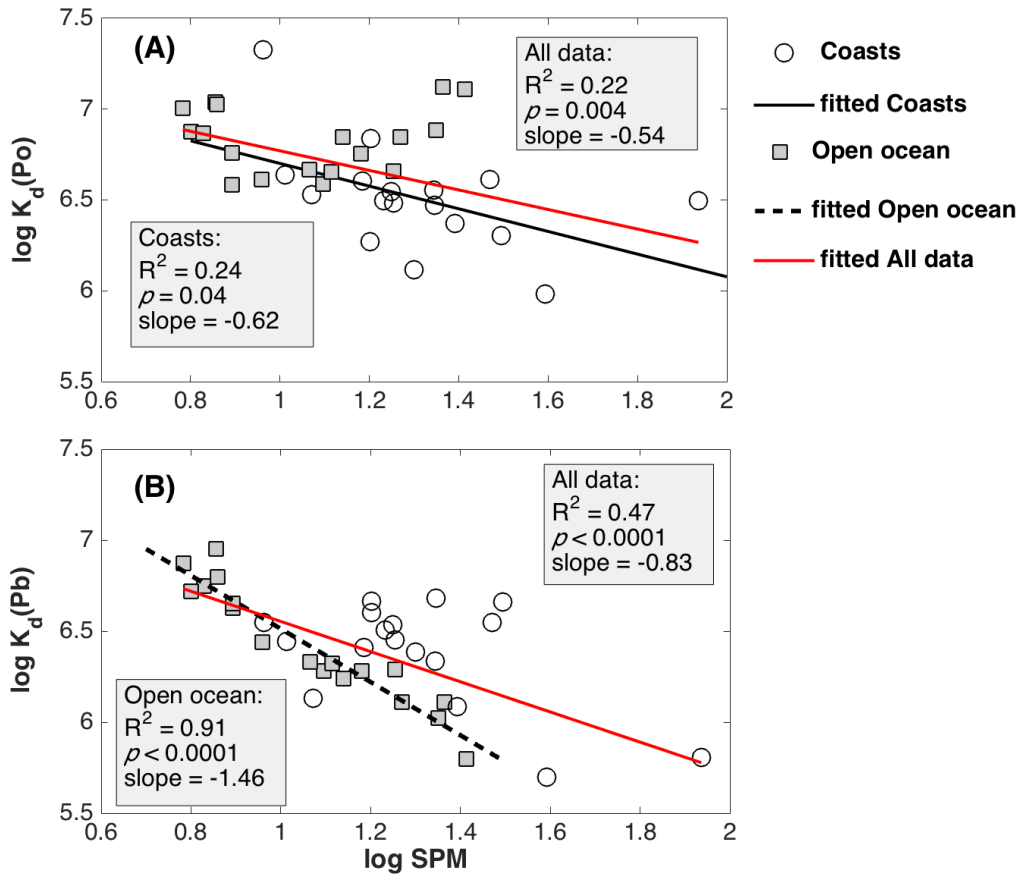

Fig. 8. The variation in the solid/solution partitioning (log K_d in L kg^{-1}) for ^{210}Po and ^{210}Pb with particle concentration (log SPM in µg L^{-1}) in the small size fraction from the upper 500 m. (A): log K_d(Po) vs. log SPM. (B): log K_d(Pb) vs. log SPM. The open circles indicate the field data from the three coastal stations (stn.10-1, 10-9, 11-1). The filled squares represent the data from the four open ocean stations (stn.11-10, -12, -16, -20). The black solid line represents the fit to the coastal data, the black dashed line represents the fit to the open ocean data, and the red solid line represents the fit to all data. All slopes shown are significant ($p < 0.05$).

These results suggest that the available binding sites for ^{210}Po and ^{210}Pb for a given particle concentration may be different between the coasts and open ocean along the transect, probably related to particle size, composition, and origin (Balls, 1989; Honeyman et al., 1988). This supports our previous findings in section 4.1, for example, that ^{210}Po and lithogenics were correlated at the coasts but not in the open ocean. Further, the clustering of our PCA scores in Fig. 3 suggests a more homogeneous particle composition in the open ocean and a more heterogeneous particle composition at the coasts, and the relationships between the principal components and proxies for production (SPM) and remineralization (AOU, depth) suggest different drivers for the composition of the particles.

554 **4.4.End-member mixing model evaluation: Observed vs. Predicted**

555 Based on our analyses thus far which indicates a significant difference in the drivers of
556 particle composition along our transect, we separated our proportional composition and bulk
557 K_d (SSF) dataset into coastal (n = 17) and open ocean (n = 14) stations in order to calculate
558 the partition coefficient for each end-member via non-negative least squares regression (Eq.
559 4). The significant $(K_d)_i$ values for each compositional component obtained from the
560 regression for ^{210}Po and ^{210}Pb are listed in Table 3.

561

562 Table 3. Model-predicted distribution coefficients (L kg^{-1}) for ^{210}Po ($K_d(Po)_i$) and ^{210}Pb ($K_d(Pb)_i$) for six end
563 members of particulate materials in the small size fraction (SSF) and their associated fraction factors, F(Po/Pb)
564 = $K_d(Po)/K_d(Pb)$.

	Components	$K_d(Po)$ $\times 10^7$	±	$K_d(Pb)$ $\times 10^7$	±	F(Po/Pb)	±
SSF, Coasts (n = 17)	POM	-	-	-	-	-	-
	$CaCO_3$	1.14	0.29	0.18	0.05	6.3	2.4
	Opal	-	-	3.24	0.35	-	-
	Litho	0.52	0.18	0.3	0.05	1.7	0.7
	Fe	-	-	-	-	-	-
	Mn	46.9	45.9	18.3	12.3	2.6	3.0
SSF, Open Ocean (n = 14)	POM	0.6	0.08	-	-	-	-
	$CaCO_3$	0.5	0.18	-	-	-	-
	Opal	-	-	6.3	1.86	-	-
	Litho	3.7	0.45	3.85	0.16	1.0	0.1
	Fe	2173.6	910.1	322.2	119.1	6.7	3.8
	Mn	-	-	87.3	33.2	-	-

565

566 Substituting $(K_d)_i$ values from Table 3 into Eq. 3, we can ultimately obtain the model-
567 predicted K_d value for each sample. Observed K_d vs. predicted K_d (OP) regressions were used
568 to evaluate the six-end member mixing model applied in this study. First, we did OP
569 regressions for the coastal (n = 17) and open-ocean K_d data (n = 14) separately. The analysis
570 of the coefficient of determination (R^2) revealed that 27% of the total variance was explained
571 by the regression model for $K_d(Po)$ at coasts, and 22% in the open ocean (data not shown). In
572 contrast, 57% and 94% of coastal $K_d(Pb)$ and oceanic $K_d(Pb)$ were explained by the OP
573 regression, respectively (data not shown). Then, we applied the OP regressions for the

574 combined data (n = 31) from the coasts and open ocean (Fig. 9). The results show 36% of the
575 total variance across all samples was explained by the regression model for K_d(Po) (Fig. 9A),
576 while 85% of the total variance of K_d(Pb) was explained by the regression model (Fig. 9B).
577 The regression of OP values was significant for both K_d(Po) (p = 0.0003) and K_d(Pb) (p =
578 1.16e-13); the slope of OP for K_d(Pb) was very close to 1 while the slope was further from 1
579 for K_d(Po). The model overestimated observed K_d(Po) at low values and underestimated it at
580 high values. Further, the intercept was significantly different from 0 from the OP regression
581 of K_d(Po) (1.3e+06) while the K_d(Pb) intercept was almost two orders of magnitude smaller
582 (closer to 0). By assessing R^2, the slope, and intercept of the OP regression, we think that the
583 model captured the main characteristics of variability of the observed K_d(Pb) well, while the
584 modeled K_d(Po) values were less reflective of the observed values. In other words, particle
585 composition based on these 6 phases can explain most of the variation in the observed
586 K_d(Pb), but it does not explain variation in the K_d(Po) as well, suggesting either the studied
587 particle composition here is not an important control on K_d(Po) or the model is missing one
588 or more important scavenging end members for ^{210}Po. This conclusion highlights the caution
589 which must be taken in interpretation of the end-member partition coefficients for ^{210}Po in
590 the following discussion.

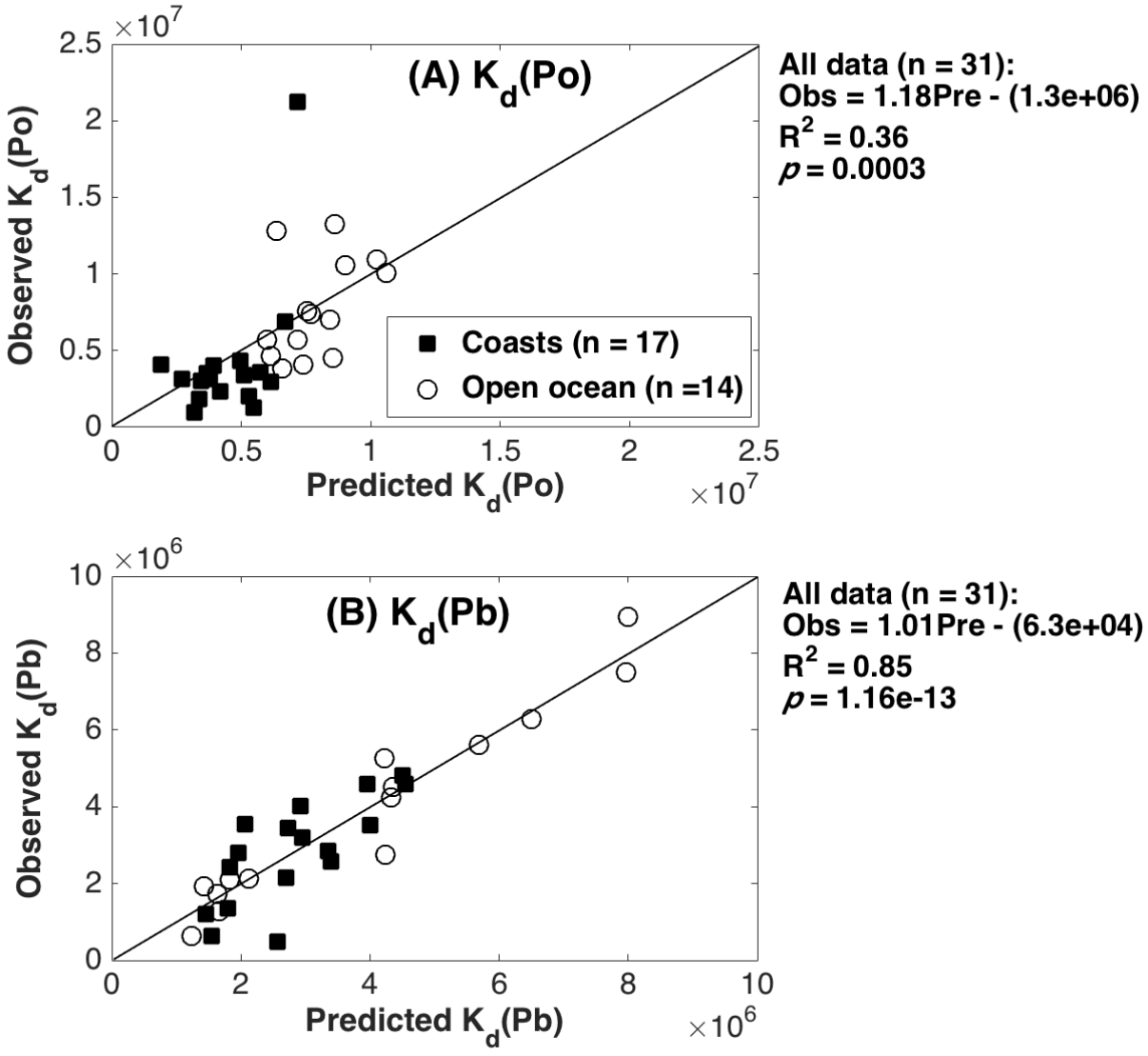

Fig. 9. Observed vs. Model predicted K_d in the small size fraction. (A) K_d(Po); (B) K_d(Pb). The filled squares and open circles represent the coastal data (n = 17) and the open ocean data (n = 14), respectively. The 1:1 line was plotted in each plot, and overall the predication captured the majority of variation in the observed K_d(Pb) while the model overestimated observed K_d(Po) at low values and underestimated it at high values. The statistical results of the regression of observed (Obs) vs. predicted (Pre) K_d values (all data, n = 31) are also shown in the graphs.

4.5.End-member partition coefficients

While we found that the end-member mixing model could predict the overall K_d(Pb) better than the overall K_d(Po), we nevertheless investigated the contribution of each phase's

partitioning strength $(K_d)_i$ to the modeled total K_d. As above, we found that the $(K_d)_i$ of each phase differed between the coast and the open ocean (e.g. $K_d(Po)_{Mn}$ for the coast was different than $K_d(Po)_{Mn}$ for the open ocean). Our results are similar to those of Li (2005) wherein the $(K_d)_i$ contribution of four measured components (lithogenic material, organic matter, carbonate, opal) for the total K_d of isotopes of Th, Pa, and Be differed between three oceanic regions. This may reflect multiple influences on $(K_d)_i$ values. The first interpretation of our results is that each measured compositional component (litho, POM, Fe, Mn, opal, and $CaCO_3$) is not chemically identical everywhere along the transect. We mentioned this above when we suggested that there may be different numbers of binding sites for a given composition and concentration of particles in the coast and open ocean.

For the lithogenic and organic (POM) components, this may reflect different elemental (e.g. Al vs. Ti vs. Fe for litho, (Ohnemus and Lam, 2015), or P content for POM (Twining et al., 2015b)) or macromolecular (e.g. differences in fatty acid or amino acid content (Stewart et al., 2007b)) composition of these *aggregated* phases from the coast to the open ocean. For the mineral phases, the measured elements (Fe, Mn, Ca, Si) may be consistent from the shore to the center of the gyre, but the organic matrices or biomolecules associated with the minerals could differ. This has been demonstrated in laboratory experiments where the organic biopolymers within mineral matrices can change the sorption nature of those minerals (Chuang et al., 2015; 2013; Yang et al., 2013).

Another possible explanation is that partition coefficients are affected by more than particle composition alone. This has been particularly noted in dynamic, coastal environments where physical and chemical conditions vary more than in the open ocean. For example, Turner (1996) highlights salinity affecting trace metal K_d values in multiple estuaries, while Balls (1989) asserts that in European coastal waters particle-particle interactions affect K_d values, justifying the need to include the SPM loadings in the calculation of K_d. That same paper asserts that previous work has found that multiple physiochemical parameters such as salinity and pH influence partition coefficients. These additional factors should be kept in mind as we detail the various $(K_d)_i$ values found for ^{210}Po and ^{210}Pb below (Table 3).

Derived end-member $K_d(Po)_i$ for the six phases were different between the coasts and open ocean. For example, Fe was not a major scavenging phase of ^{210}Po at the coasts,

whereas it was the most significant scavenger in the open ocean ($10^{10.3}$ L kg^{-1} for ^{210}Po). Mn had the opposite trend; the most significant end-member $K_d(Po)_i$ was derived from Mn at the coasts while no significant $K_d(Po)_i$ value was obtained in the open ocean. Nonetheless, the $K_d(Po)_i$ values for Mn ($10^{8.7}$ L kg^{-1}) and Fe ($10^{10.3}$ L kg^{-1}) at coastal and open ocean stations, respectively, were orders of magnitude above those for the other carrier phases in their associated oceanic regime. Previous laboratory work has also found that MnO_2 and $Fe(OH)_3$ were important in the binding of ^{210}Po (Chuang et al., 2013; Yang et al., 2013; 2015). The $K_d(Po)_i$ values for Fe and Mn reported here, though, are much larger than what has been previously reported (e.g. Fe_2O_3: $10^{4.48}$ L kg^{-1}, MnO_2: $10^{5.19}$ L kg^{-1}) (Yang et al., 2013). The above cited studies, however, did not imply that mineral phases were more important than organic phases. Instead, Chuang et al. (2013) suggested that the direct binding of ^{210}Po to organic biopolymers may be obscured due to the close association between mineral carrier phases and associated biopolymers.

There was no significant $K_d(Po)_i$ value derived for POM at the coasts, while POM was a major scavenging phase of ^{210}Po ($10^{6.8}$ L kg^{-1}) in the open ocean. This was consistent with our previous finding from the pairwise correlations and PCA analyses that there was a significant association between particulate ^{210}Po and POM at the open ocean stations but not at coastal stations. $CaCO_3$ and lithogenics, on the other hand, did not show significant difference between coasts and open ocean, with $K_d(Po)_i$ values for both carrier phases in the range of $10^{6.7} - 10^{7.6}$ L kg^{-1} in the two contrasting oceanic regimes.

Derived end-member $K_d(Pb)_i$ values for MnO_2, $CaCO_3$, lithogenics, and POM spanned 2-3 orders of magnitude. We noticed the following relationships for $K_d(Pb)$ in Table 3: K_d (Mn) > K_d (opal) > K_d (lithogenics) > K_d ($CaCO_3$) $\gg$ K_d (Fe) $\approx$ K_d (POM) = 0 at coasts; K_d (Fe) > K_d (Mn) > K_d (opal) > K_d (lithogenics) $\gg$ K_d ($CaCO_3$) $\approx$ K_d (POM) = 0 in the open ocean. The enhanced intensity of scavenging by Mn is consistent with previous work (Canfield et al., 1995; Swarzenski et al., 1999). Both studies concluded that the behavior of ^{210}Pb was tightly coupled to the redox cycling of manganese oxides, but indicated a much less significant role for iron oxides on the behavior of lead. Indeed, laboratory studies showed that MnO_2 had one order of magnitude higher K_d values for ^{210}Pb than Fe_2O_3 (Yang et al., 2013). Nevertheless, the $K_d(Pb)_i$ values for Fe ($10^{9.5}$ L kg^{-1}) and Mn ($10^{8.3\text{-}8.9}$ L kg^{-1}) derived here are much larger than what have been determined via experimental studies

(Fe_2O_3: 10^5 L kg^{-1}, MnO_2: $10^{6.3}$ L kg^{-1}) (Yang et al., 2013). This suggests that naturally formed authigenic MnO_2 may be more reactive in terms of adsorption than the pure phase that has been used in the laboratory studies. Further, the finding that $K_d(Pb)_i$ for Mn was ~100 times greater than the compositional partition coefficients for the other components (except Fe in the open ocean) appears consistent with the behavior of ^{230}Th and ^{231}Pa (Hayes et al., 2015), and that of Hg (Lamborg et al., 2016) along the same transect, but the results in those studies were either unexpected or considered a result of methods or operational definitions. Opal appeared to be another major scavenging phase of ^{210}Pb as there were significant $K_d(Pb)_i$ values ($10^{7.5}$ – $10^{7.8}$ L kg^{-1}) derived for opal from our data set. This finding supports previous work (Friedrich and Rutgers van der Loeff, 2002) and results of this study (Fig. 6), which both suggest an enhanced intensity of scavenging of ^{210}Pb by opal.

The modeled fractionation factors (F(Po/Pb)), the ratio of end-member $K_d(Po)_i$ to end-member $K_d(Pb)_i$, ranged from 1 to 6.7 in the small particles (Table 3). The end-member fractionation factors could only be derived when their associated compositional K_d's were available for both ^{210}Po and ^{210}Pb. Thus, we only obtained modeled F(Po/Pb) for $CaCO_3$, lithogenics, and Mn for coastal particles, and for lithogenics and Fe for particles in the open ocean.

We further did the OP regression of observed F(Po/Pb) vs. predicted F(Po/Pb) and found it was significant ($R^2 = 0.4$, $p = 0.0001$, data not shown). Even though the predicted $K_d(Po)$ values seemed to deviate from the observed $K_d(Po)$ values, the predicted F(Po/Pb) were relatively consistent with observed F(Po/Pb) results. We found that the strongest fractionation between ^{210}Po and ^{210}Pb was associated with coastal $CaCO_3$ (F(Po/Pb) = 6.3) and open ocean Fe (F(Po/Pb) = 6.7) showing a preference for scavenging ^{210}Po by both particulate components. The predicted fractionation factors estimated for lithogenics imply no preference for scavenging ^{210}Po over ^{210}Pb in the open ocean (F = 1), but a weak preference for ^{210}Po over ^{210}Pb at the coasts (F = 1.7).

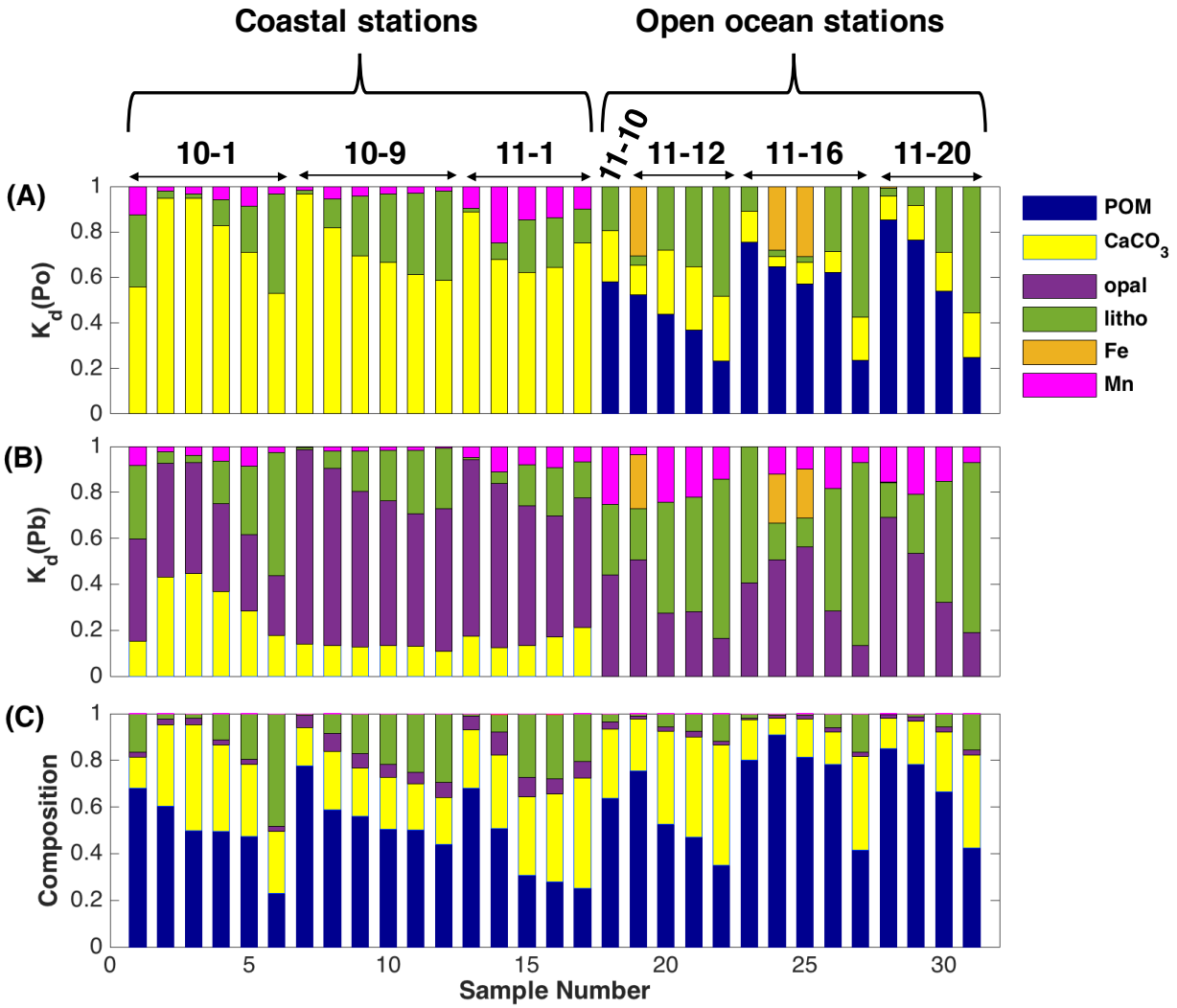

Fig. 10. The fractional contributions of six end members to the predicted bulk distribution coefficients of A) ^{210}Po (K_d(Po)), and B) ^{210}Pb (K_d(Pb)), in comparison to the weight fractions of the end members in SPM (C) in the upper 500 m. Note that there are two models applied for each K_d: one is based on coastal data (n = 17), the other is open-ocean data (n = 14). The horizontal axis represents the sample number (total 31 samples), ordered from left to right: stn.10-1 (n = 6), 10-9 (n = 6), 11-1 (n = 5), 11-10 (n = 1), 11-12 (n = 4), 11-16 (n = 5), 11-20 (n = 4) (labeled on the top of the plot).

Further, we calculated the percent contribution of each end-member to the bulk distribution coefficients to assess the importance of each end-member to scavenging (end-member K_d for phase i, $(K_d)_i$, multiplied by the percent content of phase i, f_i, divided by the total predicted K_d, $\sum f_i \cdot (K_d)_i$). Fig. 10 summarizes the percent contribution of the six EMs to the predicted partition coefficients of ^{210}Po and ^{210}Pb (Fig. 10A and B, respectively), and

the weight percent of each end member in SPM (Fig. 10C). At coastal stations, opal was the major contributor (57.1 ± 16.1%) to the predicted K_d(Pb) in the small particles, followed by $CaCO_3$ (20.3 ± 11.1%), lithogenics (17.9 ± 13.8%) and Mn (4.8 ± 3.4%). The major carrier phases of ^{210}Pb in the open ocean, in contrast, were lithogenics (43.5 ±2.0%) and opal (37.8 ± 16.8%). Further, Mn and Fe in the open ocean contributed to K_d(Pb) by 14.0 ± 7.8% and 4.8 ± 9.4%, respectively (Fig. 10B).

The contributions of the carrier phases for ^{210}Po were also different between the coasts and the open ocean; the major contributor to K_d(Po) was $CaCO_3$ (73.3 ± 14.2%) at coastal stations vs. POM (52.7 ± 20.1%) at open ocean stations. Lithogenics contributed ~ 20% to overall ^{210}Po scavenging (Fig. 10A). Interestingly, we observed Fe contributing ~ 30% and ~ 22% in 3 samples (one at stn.11-10, two at stn.11-16) for K_d(Po) and K_d(Pb), respectively, despite the low Fe concentrations of these samples (~ 0.011%). The predicted enhanced scavenging by Mn and Fe for both ^{210}Po and ^{210}Pb is surprising due to both phases' relative scarcity (low contribution to particle mass). This may highlight a bias in the derived partition coefficients for particle composition which occurs when using weight percentage rather than reactive surface area in the end-member mixing model, as suggested by Hayes et al. (2015) for Th and Pa.

4.6. ^{210}Po vs. ^{210}Pb

We observed more significant relationships between ^{210}Po and POC than between ^{210}Pb and POC, especially in the open ocean (Table 1). The positive correlation between F(Po/Pb) and %POC suggests the preference for uptake of ^{210}Po over ^{210}Pb by organic carbon and can be useful in identifying biotic vs. lithogenic particle composition, in the same manner as the ratio of ^{210}Po/^{210}Pb proposed in Radakovitch et al. (1999). A biological signature (F(Po/Pb) >1) was observed in the upper 50 m at the coastal stations and upper 300 m in the open ocean. On the other hand, F(Po/Pb) values close to or lower than unity at 100 m depth at stn.10-1, at 135 and 185 m at stn.10-9, and at 58 and 90 m at stn.11-1 suggests a more lithogenic composition, such as higher contribution from atmospheric dust or continental margin sediments. Moreover, our end member mixing analysis (EMMA) results show that K_d(Pb) for lithogenics was a factor of three higher than K_d(Pb) for POM (Table 3), further highlighting the important role of lithogenic/inorganic matter in the scavenging of ^{210}Pb. These results support the well documented preference for ^{210}Po uptake over ^{210}Pb in marine

735 organisms and that ^{210}Po is both particle-reactive and bio-reactive, whereas ^{210}Pb is only
736 particle-reactive (Fisher et al., 1983; Heyraud et al., 1976; Heyraud and Cherry, 1979; Larock
737 et al., 1996; Stewart and Fisher, 2003; Wilson et al., 2009). The known bio-reactive behavior
738 of ^{210}Po and its association with sulfur (Balistrieri et al., 1995; Cherrier et al., 1995; Harada
739 et al., 1989), both suggest its cycling in particles is more complicated than ^{210}Pb cycling and
740 supports our hypothesis that important end-members were missing for the model of K_d(Po).
741 The PCA results also support this conclusion because there was a closer association between
742 ^{210}Po and AOU than between ^{210}Pb and AOU, indicating that biological processes affect the
743 cycling of polonium more than that of lead.
744 An alternative interpretation of the less predictive power of the EMMA for ^{210}Po, the
745 model K_d(Po) values differing from the observed K_d(Po) values, was suggested in the
746 methods when we indicated that the uptake of ^{210}Po by particles is not purely due to
747 adsorption to particle surfaces as is the nature of ^{210}Pb uptake. ^{210}Po can be found associated
748 with particles via three routes: 1) direct sorption of ^{210}Po to particle surfaces, 2) the ingrowth
749 of ^{210}Po from previously sorbed ^{210}Pb, and 3) the bioconcentration and biomagnification of
750 ^{210}Po by organisms. This does not mean that K_d(Po) has no significance, meaning, or use, it
751 may, instead, explain why composition alone could not determine K_d(Po) in this study. It
752 would be nearly impossible to distinguish the relative contribution of these three pathways,
753 but this is an avenue of research that should be pursued. While we cannot easily model the
754 three processes listed above, together they will still result in a higher K_d(Po) than K_d(Pb) for
755 most samples, especially biogenic particles, so the fractionation of the two isotopes can still
756 be used to trace the export of particles.
757 **5. Conclusions**
758 From an investigation into the partitioning of ^{210}Po and ^{210}Pb activity between particles
759 and solution in the upper 500 m water column across the North Atlantic basin, and an
760 analysis of how the particle concentration and composition affect their partitioning, we draw
761 the following conclusions:
762 (1) While both K_d(Po) and K_d(Pb) were inversely related to particle concentration, their
763 relationships differed between the coasts and open ocean, and the particle
764 concentration effect was strongest for K_d(Pb) in the open ocean.

(2) Our correlation and PCA results indicated that the relationships between ^{210}Po and ^{210}Pb activity and the composition of coastal and open ocean particles were different, but that particle concentration (SPM), remineralization/residence time (AOU), and depth were important drivers of variability in both small and large particles.

(3) A six-end member particle composition mixing model could accurately predict the scavenging of ^{210}Pb, and indicated that opal and lithogenic phases are the major drivers of K_d(Pb). The mixing model could not predict K_d(Po) with as much accuracy, indicating either that the model is missing important scavenging end members for ^{210}Po, (such as sulfur, protein, or another component of organic matter) or that particle composition alone is not the only driver of K_d(Po) because the partitioning of ^{210}Po between the dissolved and particulate phase is more complicated than simple sorption.

(4) Despite the complexity of the cycling of ^{210}Po and ^{210}Pb, and the diversity of particle concentration and composition measured along the GEOTRACES North Atlantic Zonal Transect (GA03), ^{210}Po consistently exhibited a higher affinity for POC than ^{210}Pb, supporting the use of ^{210}Po fractionation and disequilibrium from ^{210}Pb, as a tracer of the export of organic matter in the surface ocean.

Acknowledgements

We thank Captain Adam Seamans, the crew of the R/V Knorr, and the chief scientists of the GA03 cruise (B. Jenkins, E. Boyle, and G. Cutter). Special thanks to the science team samplers for the Niskin bottles and in situ pumps (Chris Hayes, Katharina Pahnke, Brett Longworth, Paul Morris, Daniel Ohnemus, Steven Spike, Kuanbo Zhou, and Stephanie Owens) for helping at sea. On-shore radiochemical analysis efforts of Hiu-Yan Choi, Judith Sarkodee-Adoo, and Anupam Kumar are greatly appreciated. We also want to acknowledge the contribution of analyses and data from the Baskaran laboratory at Wayne State University. Funding for ship time, sampling operations, and hydrographic data was supported by the U.S. National Science Foundation to the US GEOTRACES North Atlantic Transect Management team of W. Jenkins (OCE-0926423), E. Boyle (OCE-0926204), and G. Cutter (OCE-0926092). This work was funded by grants from the NSF to T. Church (OCE-0961653), M. Baskaran (OCE-0961351) and G. Stewart (OCE-0960924).

References:

Abramson, L., Lee, C., Wakeham, S.G., Szlosek, J., 2010. Exchange between suspended and sinking particles in the northwest Mediterranean as inferred from the organic composition of in situ pump and sediment trap samples. Limnology and Oceanography 55.

Armstrong, R.A., Lee, C., Hedges, J.I., Honjo, S., Wakeham, S.G., 2001. A new, mechanistic model for organic carbon fluxes in the ocean based on the quantitative association of POC with ballast minerals. Deep Sea Research Part II 49, 219–236.

Bacon, M.P., Spencer, D.W., Brewer, P.G., 1976. 210Pb/226Ra and 210Po/210Pb disequilibria in seawater and suspended particulate matter. Earth and Planetary Science Letters 32, 277–296.

Balistrieri, L.S., Murray, J.W., Paul, B., 1995. The geochemical cycling of stable Pb, 210Pb, and 210Po in seasonally anoxic Lake Sammamish, Washington, USA. GCA 59, 4845–4861.

Balls, P.W., 1989. The partition of trace metals between dissolved and particulate phases in european coastal waters: A compilation of field data and comparison with laboratory studies. Netherlands Journal of Sea Research 23, 7–14.

Baskaran, M., Santschi, P.H., 1993. The role of particles and colloids in the transport of radionucldies in coastal environments of Texas. Marine Chemistry 43, 95–114.

Baskaran, M., Santschi, P.H., Benoit, G., Honeyman, B.D., 1992. Scavenging of thorium isotopes by colloids in seawater of the Gulf of Mexico. GCA 56, 3375–3388.

Benoit, G., Rozan, T.F., 1999. The influence of size distribution on the particle concentration effect and trace metal partitioning in rivers. GCA 63, 113–127.

Bibby, T.S., Gorbunov, M.Y., Wyman, K.W., Falkowski, P.G., 2008. Photosynthetic community responses to upwelling in mesoscale eddies in the subtropical North Atlantic and Pacific Oceans. Deep Sea Research Part II 55, 1310–1320.

Buesseler, K.O., Bacon, M.P., Kirk Cochran, J., Livingston, H.D., 1992. Carbon and nitrogen export during the JGOFS North Atlantic Bloom experiment estimated from 234Th: 238U disequilibria. Deep-Sea Research Part A-Oceanographic Research Papers 39, 1115–1137.

Buesseler, K.O., Lamborg, C., Cai, P., Escoube, R., Johnson, R., Pike, S., Masqué, P., McGillicuddy, D., Verdeny, E., 2008. Particle fluxes associated with mesoscale eddies in the Sargasso Sea. Deep Sea Research Part II 55, 1426–1444. doi:10.1016/j.dsr2.2008.02.007

Canfield, D.E., Green, W.J., Nixon, P., 1995. 210Pb and stable lead through the redox transition zone of an Antarctic lake. GCA 59, 2459–2468.

Carvalho, F.P., 2011. Polonium (210Po) and lead (210Pb) in marine organisms and their transfer in marine food chains. International Topical Meeting on Polonium and Radioactive Lead Isotopes 102, 462–472.

Charette, M.A., Moran, S.B., Pike, S.M., Smith, J.N., 2001. Investigating the carbon cycle in the Gulf of Maine using the natural tracer thorium 234. J. Geophys. Res. 106, 11553–11579. doi:10.1029/1999JC000277

Chase, Z., Anderson, R.F., Fleisher, M.Q., Kubik, P.W., 2002. The influence of particle composition and particle flux on scavenging of Th, Pa and Be in the ocean. Earth and Planetary Science Letters 204, 215–229.

Cherrier, J., Burnett, W.C., LaRock, P.A., 1995. Uptake of polonium and sulfur by bacteria. Geomicrobiology Journal 13, 103–115. doi:10.1080/01490459509378009

Chuang, C., Santschi, P.H., Ho, Y., Conte, M.H., Guo, L., Schumann, D., Ayranov, M., Li, Y.,

2013. Role of biopolymers as major carrier phases of Th, Pa, Pb, Po, and Be radionuclides in settling particles from the Atlantic Ocean. Biogeochemistry of trace elements and their isotopes 157, 131–143.
Chuang, C., Santschi, P.H., Jiang, Y., Ho, Y., Quigg, A., Guo, L., Ayranov, M., Schumann, D., 2014. Important role of biomolecules from diatoms in the scavenging of particle-reactive radionuclides of thorium, protactinium, lead, polonium, and beryllium in the ocean: A case study with Phaeodactylum tricornutum. Limnology and Oceanography 59, 1256–1266. doi:10.4319/lo.2014.59.4.1256
Chuang, C., Santschi, P.H., Wen, L., Guo, L., Xu, C., Zhang, S., Jiang, Y., Ho, Y., Schwehr, K.A., Quigg, A., Hung, C., Ayranov, M., Schumann, D., 2015. Binding of Th, Pa, Pb, Po and Be radionuclides to marine colloidal macromolecular organic matter. Biogeochemistry of trace elements and their isotopes 173, 320–329.
Clegg, S.L., Whitfield, M., 1991. A generalied model for the scavenging of trace metals in the open ocean-II. Thorium scavenging. Deep-Sea Research Part A-Oceanographic Research Papers 38, 91–120.
Clegg, S.L., Whitfield, M., 1990. A generalised model for the scavenging of trace metals in the open ocean: I. Particle cycling. Deep-Sea Research Part A-Oceanographic Research Papers 37, 809–832.
Cochran, J.K., 2003. Short-lived U/Th Series Radionuclides in the Ocean: Tracers for Scavenging Rates, Export Fluxes and Particle Dynamics. Reviews in Mineralogy and Geochemistry 52, 461–492. doi:10.2113/0520461
Cutter, G.A., Andersson, P., Codispoti, L., Francois, R., Croot, P., Lohan, M., Obata, H., Rutgers van der Loeff, M.M., 2010. Sampling and Sample-handling Protocols for GEOTRACES Cruises [WWW Document]. URL http://www.geotraces.org/libraries/documents/Intercalibration/Cookbook.pdf (accessed 4.19.16).
Djogic, R., Sipos, L., Branica, M., 1986. Characterization of uranium(V1) in seawater. Limnology and Oceanography 31, 1122–1131. doi:10.4319/lo.1986.31.5.1122
Duteil, O., Koeve, W., Oschlies, A., Bianchi, D., Galbraith, E., Kriest, I., Matear, R., 2013. A novel estimate of ocean oxygen utilisation points to a reduced rate of respiration in the ocean interior. BG 10, 7723–7738.
Efron, B., Stein, C., 1981. The Jackknife estimate of variance. The Annals of Statistics 9, 586–596.
Fisher, N.S., Burns, K.A., Cherry, R.D., Heyraud, M., 1983. Accumulation and cellular distribution of ^{241}Am, ^{210}Po and ^{210}Pb in two marine algae. Marine Ecology Progress Series 11, 233–237.
Friedrich, J., Rutgers van der Loeff, M.M., 2002. A two-tracer (210Po–234Th) approach to distinguish organic carbon and biogenic silica export flux in the Antarctic Circumpolar Current. Deep Sea Research Part I: Oceanographic Research Papers 49, 101–120.
Harada, K., Burnett, W.C., LaRock, P.A., Cowart, J.B., 1989. Polonium in Florida groundwater and its possible relationship to the sulfur cycle and bacteria. GCA 53, 143–150.
Hayes, C.T., Anderson, R.F., Fleisher, M.Q., Vivancos, S.M., Lam, P.J., Ohnemus, D.C., Huang, K., Robinson, L.F., Lu, Y., Cheng, H., Edwards, R.L., Moran, S.B., 2015. Intensity of Th and Pa scavenging partitioned by particle chemistry in the North Atlantic Ocean. Biogeochemistry of trace elements and their isotopes 170 IS -, 49–60.
Heyraud, M., Cherry, R.D., 1979. Polonium-210 and lead-210 in marine food chains. Mar. Biol.

52, 227–236. doi:10.1007/BF00398136
Heyraud, M., Fowler, S.W., Beasley, T.M., Cherry, R.D., 1976. Polonium-210 in euphausiids: A detailed study. Mar. Biol. 34, 127–136. doi:10.1007/BF00390754
Honeyman, B.D., Balistrieri, L.S., Murray, J.W., 1988. Oceanic trace metal scavenging: the importance of particle concentration. Deep-Sea Research Part A-Oceanographic Research Papers 35, 227–246.
Honeyman, B.D., Santschi, P.H., 1989. A Brownian-pumping model for oceanic trace metal scavenging: Evidence from Th isotopes. Journal of Marine Research 47, 951–992. doi:10.1357/002224089785076091
Hong, G.-H., Park, S.-K., Baskaran, M., Kim, S.-H., Chung, C.-S., Lee, S.-H., 1999. Lead-210 and polonium-210 in the winter well-mixed turbid waters in the mouth of the Yellow Sea. Continental Shelf Research 19, 1049–1064. doi:10.1016/S0278-4343(99)00011-4
Ito, T., Follows, M.J., Boyle, E.A., 2004. Is AOU a good measure of respiration in the oceans? Geophysical Research Letters 31, n/a–n/a. doi:10.1029/2004GL020900
Kharkar, D.P., Tiiomson, J., Turekian, K.K., Forster, W.O., 1976. Uranium and thorium decay series nuclides in plankton from the Caribbean. Limnology and Oceanography 21, 294–299. doi:10.4319/lo.1976.21.2.0294
Kohler, U., Luniak, M., 2005. Data inspection using biplots. Stata Journal 5, 208–223.
Lam, P.J., Ohnemus, D.C., Auro, M.E., 2015. Size-fractionated major particle composition and concentrations from the US GEOTRACES North Atlantic Zonal Transect. Deep Sea Research Part II 116, 303–320. doi:10.1016/j.dsr2.2014.11.020
Lamborg, C.H., Hammerschmidt, C.R., Bowman, K.L., 2016. An examination of the role of particles in oceanic mercury cycling. Phil. Trans. R. Soc. A 374, 20150297. doi:10.1098/rsta.2015.0297
Larock, P., Hyun, J.H., Boutelle, S., Burnett, W.C., Hull, C.D., 1996. Bacterial mobilization of polonium. GCA 60, 4321–4328.
Le Moigne, F.A.C., Villa-Alfageme, M., Sanders, R.J., Marsay, C., Henson, S., García-Tenorio, R., 2013. Export of organic carbon and biominerals derived from 234Th and 210Po at the Porcupine Abyssal Plain. Deep Sea Research Part I: Oceanographic Research Papers 72, 88–101.
Lepore, K., Moran, S.B., Burd, A.B., Jackson, G.A., Smith, J.N., Kelly, R.P., Kaberi, H., Stavrakakis, S., Assimakopoulou, G., 2009. Sediment trap and in-situ pump size-fractionated POC/234Th ratios in the Mediterranean Sea and Northwest Atlantic: Implications for POC export. Deep Sea Research Part I: Oceanographic Research Papers 56, 599–613.
Lerner, P., Marchal, O., Lam, P.J., Buesseler, K., Charette, M., 2017. Kinetics of thorium and particle cycling along the U.S. GEOTRACES North Atlantic Transect. Deep Sea Research Part I: Oceanographic Research Papers. doi:10.1016/j.dsr.2017.05.003
Li, Y., 2005. Controversy over the relationship between major components of sediment-trap materials and the bulk distribution coefficients of 230Th, 231Pa, and 10Be. Earth and Planetary Science Letters 233, 1–7.
Masqué, P., Sanchez-Cabeza, J.A., Bruach, J.M., Palacios, E., Canals, M., 2002. Balance and residence times of 210Pb and 210Po in surface waters of the northwestern Mediterranean Sea. Continental Shelf Research 22, 2127–2146. doi:10.1016/S0278-4343(02)00074-2
Murray, J.W., Paul, B., Dunne, J.P., Chapin, T., 2005. 234Th, 210Pb, 210Po and stable Pb in the central equatorial Pacific: Tracers for particle cycling. Deep Sea Research Part I: Oceanographic Research Papers 52, 2109–2139.

Nozaki, Y., Dobashi, F., Kato, Y., Yamamoto, Y., 1998. Distribution of Ra isotopes and the 210Pb and 210Po balance in surface seawaters of the mid Northern Hemisphere. Deep Sea Research Part I: Oceanographic Research Papers 45, 1263–1284. doi:10.1016/S0967-0637(98)00016-8

Ohnemus, D.C., Lam, P.J., 2015. Cycling of lithogenic marine particles in the US GEOTRACES North Atlantic transect. Deep Sea Research Part II 116, 283–302. doi:10.1016/j.dsr2.2014.11.019

Quigley, M.S., Santschi, P.H., Hung, C., Guo, L., Honeyman, B.D., 2002. Importance of acid polysaccharides for 234Th complexation to marine organic matter. Limnology and Oceanography 47, 367–377. doi:10.4319/lo.2002.47.2.0367

Radakovitch, O., Cherry, R.D., Heussner, S., 1999. 210Pb and 210Po: tracers of particle transfer on the Rhône continental margin (NW Mediterranean). Deep Sea Research Part I: Oceanographic Research Papers 46, 1539–1563.

Rigaud, S., Stewart, G., Baskaran, M., Marsan, D., Church, T., 2015. 210Po and 210Pb distribution, dissolved-particulate exchange rates, and particulate export along the North Atlantic US GEOTRACES GA03 section. Deep Sea Research Part II 116, 60–78. doi:10.1016/j.dsr2.2014.11.003

Savoye, N., Benitez-Nelson, C., Burd, A.B., Cochran, J.K., Charette, M., Buesseler, K.O., Jackson, G.A., Roy-Barman, M., Schmidt, S., Elskens, M., 2006. 234Th sorption and export models in the water column: A review. Biogeochemistry of trace elements and their isotopes 100, 234–249.

Shannon, L.V., Cherry, R.D., Orren, M.J., 1970. Polonium-210 and lead-210 in the marine environment. GCA 34, 701–711.

Shimmield, G.B., Ritchie, G.D., Fileman, T.W., 1995. The impact of marginal ice zone processes on the distribution of 21OPb, 21OPo and 234Th and implications for new production in the Bellingshausen Sea, Antarctica. Deep Sea Research Part II 42, 1313–1335.

Stanley, R.H.R., Doney, S.C., Jenkins, W.J., Lott, D.E.I., 2012. Apparent oxygen utilization rates calculated from tritium and helium-3 profiles at the Bermuda Atlantic Time-series Study site. Biogeosciences 9, 1969–1983.

Stewart, G., Cochran, J.K., Miquel, J.C., Masqué, P., Szlosek, J., Rodriguez y Baena, A.M., Fowler, S.W., Gasser, B., Hirschberg, D.J., 2007a. Comparing POC export from 234Th/238U and 210Po/210Pb disequilibria with estimates from sediment traps in the northwest Mediterranean. Deep Sea Research Part I: Oceanographic Research Papers 54, 1549–1570. doi:10.1016/j.dsr.2007.06.005

Stewart, G., Kirk Cochran, J., Xue, J., Lee, C., Wakeham, S.G., Armstrong, R.A., Masqué, P., Carlos Miquel, J., 2007b. Exploring the connection between 210Po and organic matter in the northwestern Mediterranean. Deep Sea Research Part I: Oceanographic Research Papers 54, 415–427. doi:10.1016/j.dsr.2006.12.006

Stewart, G.M., Fisher, N.S., 2003. Bioaccumulation of polonium-210 in marine copepods. Limnology and Oceanography 48, 2011–2019. doi:10.4319/lo.2003.48.5.2011

Stewart, G.M., Fowler, S.W., Teyssié, J.L., Cotret, O., Cochran, J.K., Fisher, N.S., 2005. Contrasting transfer of polonium-210 and lead-210 across three trophic levels in marine plankton. Marine Ecology Progress Series 290, 27–33. doi:10.3354/meps290027

Su, K., Du, J., Baskaran, M., Zhang, J., 2016. 210Po and 210Pb disequilibrium at the PN section in the East China Sea. International Topical Meeting on Polonium and Radioactive Lead Isotopes.

Swarzenski, P.W., McKee, B.A., Sørensen, K., Todd, J.F., 1999. 210Pb and 210Po, manganese and iron cycling across the O2/H2S interface of a permanently anoxic fjord: Framvaren, Norway. Biogeochemistry of trace elements and their isotopes 67, 199–217.
Theng, T.L., Mohamed, C.A.R., 2005. Activities of 210Po and 210Pb in the water column at Kuala Selangor, Malaysia. International Topical Meeting on Polonium and Radioactive Lead Isotopes 80, 273–286.
Turner, A., 1996. Trace-metal partitioning in estuaries: importance of salinity and particle concentration. Biogeochemistry of trace elements and their isotopes 54, 27–39.
Twining, B.S., Rauschenberg, S., Morton, P.L., Vogt, S., 2015a. Metal contents of phytoplankton and labile particulate material in the North Atlantic Ocean. Progress in Oceanography 137, 261–283. doi:10.1016/j.pocean.2015.07.001
Twining, B.S., Rauschenberg, S., Morton, P.L., Vogt, S., 2015b. Metal contents of phytoplankton and labile particulate material in the North Atlantic Ocean. Progress in Oceanography 137, 261–283.
Verdeny, E., Masqué, P., Garcia-Orellana, J., Hanfland, C., Kirk Cochran, J., Stewart, G.M., 2009. POC export from ocean surface waters by means of 234Th/238U and 210Po/210Pb disequilibria: A review of the use of two radiotracer pairs. Deep Sea Research Part II 56, 1502–1518. doi:10.1016/j.dsr2.2008.12.018
Verdeny, E., Masqué, P., Maiti, K., Garcia-Orellana, J., Bruach, J.M., Mahaffey, C., Benitez-Nelson, C.R., 2008. Particle export within cyclonic Hawaiian lee eddies derived from 210Pb–210Po disequilibrium. Deep Sea Research Part II: Topical Studies in Oceanography 55, 1461–1472. doi:10.1016/j.dsr2.2008.02.009
Wakeham, S.G., Canuel, E.A., 1988. Organic geochemistry of particulate matter in the eastern tropical North Pacific Ocean: Implications for particle dynamics. Journal of Marine Research 46, 183–213. doi:doi:10.1357/002224088785113748
Wei, C., Lin, S., Wen, L., Sheu, D.D.D., 2012. Geochemical behavior of 210Pb and 210Po in the nearshore waters off western Taiwan. Marine Pollution Bulletin 64, 214–220.
Wei, C., Murray, J.W., 1994. The behavior of scavenged isotopes in marine anoxic environments: 210Pb and 210Po in the water column of the Black Sea. GCA 58, 1795–1811.
Wei, C.L., Yi, M.C., Lin, S.Y., Wen, L.S., Lee, W.H., 2014. Seasonal distributions and fluxes of 210Pb and 210Po in the northern South China Sea. Biogeosciences 11, 6813–6826.
Wilson, R.C., Watts, S.J., Vives i Batlle, J., McDonald, P., 2009. Laboratory and field studies of polonium and plutonium in marine plankton. International Topical Meeting on Polonium and Radioactive Lead Isotopes 100, 665–669.
Yang, W., Guo, L., Chuang, C., Santschi, P.H., Schumann, D., Ayranov, M., 2015. Influence of organic matter on the adsorption of 210Pb, 210Po and 7Be and their fractionation on nanoparticles in seawater. Earth and Planetary Science Letters 423, 193–201.
Yang, W., Guo, L., Chuang, C., Schumann, D., Ayranov, M., Santschi, P.H., 2013. Adsorption characteristics of 210Pb, 210Po and 7Be onto micro-particle surfaces and the effects of macromolecular organic compounds. GCA 107, 47–64.